Avoidance of hydrogen sulfide is modulated by external and internal states in *C. elegans*

Longjun Pu[1, 2, 3], Lina Zhao[1, 2, 3], Jing Wang[1, 2, 3], Clementine Deleuze[6], Lars Nilsson[1, 2, 3], Johan Henriksson[1, 4, 5], Patrick Laurent[6*], Changchun Chen[1, 2, 3*]

[1]Department of Molecular Biology, Umeå University, Umeå, Sweden

[2]Umeå Centre for Molecular Medicine, Umeå University, Umeå, Sweden

[3]Wallenberg Centre for Molecular Medicine, Umeå University, Umeå, Sweden

[4]The Laboratory for Molecular Infection Medicine Sweden (MIMS), Umeå University, Umeå, Sweden

[5]Integrated Science Lab (Icelab), Umeå University, Umeå, Sweden

[6]Laboratory of Neurophysiology, ULB Neuroscience Institute (UNI), Université Libre de Bruxelles (ULB), Belgium

*Corresponding author

E-mail: patrick.laurent.ulb@gmail.com; Changchun.chen@umu.se

Abstract

Hydrogen sulfide (H_2S) acts as an energy source, a toxin, and a gasotransmitter across diverse biological contexts. We use the robust locomotory responses of *Caenorhabditis elegans* to high levels of H_2S to elucidate the molecular mechanisms underlying its acute and adaptive responses. We find that the H_2S-evoked behavioral response is shaped by multiple environmental factors including oxygen (O_2) levels and nutritional state, and is modulated by various pathways such as insulin, TGF-β, and HIF-1 signaling, as well as by input from O_2-sensing neurons. Prolonged exposure to H_2S activates HIF-1 signaling, leading to the upregulation of stress-responsive genes, including those involved in H_2S detoxification. This promotes an adaptive state in which locomotory speed is reduced in H_2S, while responsiveness to other stimuli is preserved. In mutants deficient in HIF-1 signaling, iron storage, and detoxification mechanisms, animals display a robust initial response but rapidly enter a sleep-like behavior characterized by reduced mobility and diminished responsiveness to subsequent sensory stimuli. Furthermore, while acute production of mitochondria-derived reactive O_2 species (ROS) appears to initiate the avoidance response to H_2S, persistently high ROS promotes an adaptive state, likely by activating various stress-response pathways, without substantially compromising cellular H_2S detoxification capacity. Taken together, our study provides comprehensive molecular insights into the mechanisms through which *C. elegans* modulates and adapts its response to H_2S exposure.

Introduction

During the late Proterozoic era, the rise in oxygen (O_2) levels eliminated hydrogen sulfide (H_2S) from most habitats. Yet, low O_2 levels, along with high concentrations of hydrogen sulfide (H_2S) and carbon dioxide (CO_2), can persist in enclosed environments where bacteria actively decompose organic matter (Olson & Straub, 2016). H_2S can easily permeate biological membranes and interfere with various cellular processes. One of the most detrimental effects of H_2S is the disruption of cellular respiration by remodeling the mitochondrial electron transport chain and inhibiting cytochrome *c* oxidase (COX) (Cooper & Brown, 2008; Khan et al., 1990; Nicholls & Kim, 1982; Romanelli-Cedrez, Vairoletti, & Salinas, 2024).

The detection and response to chemical signals are crucial for various organisms to interact effectively with their environment. Animals living in H_2S-rich environments have evolved mechanisms to either avoid or adapt to these conditions, conferring them survival advantages. Species that encounter periodic increases in H_2S often exhibit avoidance behaviors. For example, benthic species undertake daily vertical migrations between sulfidic and non-sulfidic waters (Abel, Koenig, & Davis, 1987; Salvanes, Utne-Palm, Currie, & Braithwaite, 2011). Certain metazoan species have seized the ecological opportunities presented by H_2S-rich environments through the development of cellular adaptations. Livebearing fish species, for instance, have evolved COX subunits that are more resistant to H_2S and more efficient at H_2S detoxification (Kelley et al., 2016; Pfenninger et al., 2014).

Free-living nematodes feed on bacteria that thrive in decaying organic matter, such as compost. This complex and dynamic environment, where species like *C. elegans* are commonly found, may exhibit significant fluctuations in H_2S levels over short distances (Adams, Farwell, Pack, & Bamesberger, 1979; Budde & Roth, 2011; Morra & Dick, 1991; Patange, Breen, Arsuffi, & Ruvkun, 2025; Rodriguez-Kabana, Jordan, & Hollis, 1965; Romanelli-Cedrez et al., 2024). Evidence suggests that *C. elegans* has evolved tolerance to prolonged H_2S exposure by reprogramming gene expression through H_2S-induced stabilization of the hypoxia-inducible factor HIF-1 (Budde & Roth, 2010, 2011; Horsman, Heinis, & Miller, 2019; Ma, Vozdek, Bhatla, & Horvitz, 2012; Miller, Budde, & Roth, 2011; Powell-Coffman, 2010; Topalidou &

65 Miller, 2017), and by developing an H_2S-resistant electron transport chain (Romanelli-Cedrez
66 et al., 2024). In particular, low concentrations of H_2S are not only well tolerated but can also
67 be beneficial. For instance, exposure to 50 ppm H_2S has been shown to extend the lifespan and
68 enhance thermotolerance (Fawcett, Hoyt, Johnson, & Miller, 2015; Miller & Roth, 2007).
69 Moreover, endogenous H_2S production in *C. elegans* modulates its interactions with
70 actinobacteria (Patange et al., 2025). However, exposure to concentrations exceeding 150 ppm
71 proved lethal (Budde & Roth, 2010; Horsman et al., 2019).

72 In addition to long-term adaptive mechanisms, *C. elegans* exhibits an acute behavioral
73 response to H_2S exposure (Budde & Roth, 2011). In this study, we investigated whether and
74 how the nematode *C. elegans* acutely avoids environments rich in H_2S, how it adapts at the
75 molecular and physiological levels to H_2S exposure, and how these adaptations alter the
76 avoidance response.

77

78 **Results**

79 ***C. elegans* increases locomotory activity in response to acute H_2S exposure**

80 In response to aversive cues, *C. elegans* initiates a pirouette followed by an increase of its
81 locomotory speed to escape the noxious stimuli. When acutely exposed to 150 ppm H_2S, the
82 laboratory N2 strain exhibited an increased locomotory speed and enhanced turning behavior,
83 while generally decreasing the frequency of reversals, as a strategy to escape the noxious
84 stimuli (***Figure 1A–C, Figure 1—Video 1***). The maximum speed was reached after 6–8
85 minutes in H_2S and returned to the baseline over a period of approximately 1 hour (***Figure 1D***).
86 The reduced locomotory speed after 30 minutes in 150 ppm H_2S was reversible when these
87 animals were immediately challenged with another stimulus, such as near-UV light (***Figure***
88 ***1E***), suggesting that neuromuscular function remains preserved. The magnitude and dynamics
89 of the H_2S-induced avoidance responses were concentration-dependent. Under our assay
90 conditions, 50 ppm H_2S did not elicit an acute speed increase, and responses to 75 ppm were
91 variable. In contrast, exposure to 150 ppm H_2S consistently triggered a robust and reproducible
92 escape response (***Figure 1F***), consistent with earlier reports that H_2S at 50 ppm exerts

93 beneficial effects, while H_2S at 150 ppm is toxic to *C. elegans* (Budde & Roth, 2010; Fawcett
94 et al., 2015; Horsman et al., 2019; Miller & Roth, 2007). To investigate whether low levels of
95 H_2S might be preferable or even attractive to the animals, we exposed wild type animals to a
96 linear gradient of H_2S (***Figure 1G***; See methods for details) (Bretscher, Busch, & de Bono,
97 2008; Chang, Chronis, Karow, Marletta, & Bargmann, 2006; Gray et al., 2004). Animals were
98 allowed to move freely on a thin layer of bacteria within a microfluidic chamber containing an
99 H_2S gradient ranging from 150 ppm at one end to 0 ppm at the other. As expected, *C. elegans*
100 robustly avoids 150 ppm H_2S but does not accumulate at the extreme end of 0 ppm ***(Figure 1G,***
101 ***H).*** The highest proportion of animals was found in the region with approximately 40 ppm H_2S.
102 These data suggest that H_2S acts as a potent repellent for *C. elegans* at high concentrations but
103 as an attractant at low levels.
104
105 **Candidate gene screen identifies signaling pathways required for H_2S-evoked locomotion**
106 To investigate the molecular mechanisms underlying the H_2S-evoked locomotory response in
107 *C. elegans*, we conducted a candidate gene screen for mutants that failed to increase their
108 locomotory speed upon exposure to an acute rise of H_2S level to 150 ppm. Our analysis
109 prioritized genes that are either known to be, or potentially involved in, sensory responses to
110 gaseous stimuli in both *C. elegans* and mammals (***Supplementary file 1***). We began by
111 examining mutants affecting globins, guanylate cyclases, and cyclic nucleotide-gated (CNG)
112 channels, which are involved in O_2 or CO_2 sensing in *C. elegans*, as well as wild isolates and
113 other previously characterized mutants with defective responses to gas stimuli (***Supplementary***
114 ***file 1***) (Bretscher et al., 2008; Gray et al., 2004; Hallem & Sternberg, 2008; Persson et al., 2009).
115 Given the essential role of K^+ channels in acute hypoxia sensing in mammals, we also screened
116 all potassium (K^+) channel mutants (Gao, Gonzalez-Rodriguez, Ortega-Saenz, & Lopez-Barneo,
117 2017; Weir, Lopez-Barneo, Buckler, & Archer, 2005). To explore the neuronal components
118 involved in H_2S-evoked avoidance, we assayed mutants with defects in ciliogenesis or cilia-
119 mediated signaling, as well as animals deficient in neurotransmission involving classical
120 neurotransmitters, neuropeptides, or biogenic amines. Finally, considering that mitochondrial

121 function is central to H_2S detoxification, we included mitochondrial electron transport chain
122 (ETC) mutants and key factors implicated in H_2S and superoxide clearance. Together, these
123 functionally diverse categories allowed us to survey a wide spectrum of potential mechanisms
124 contributing to the behavioral response to H_2S.

125 In the screen, a collection of mutants displayed reduced speed response, whereas only
126 a few exhibited a lack of omega-turn and/or reversal responses to H_2S (***Supplementary file 1***).
127 The reversal inhibition upon H_2S exposure and its rebound following H_2S withdrawal appeared
128 to vary substantially across experiments for N2, suggesting that differences in population
129 density, food availability, and animals' physiological state prior to the assay may matter.
130 Nevertheless, our screen revealed that signaling pathways, including cGMP, insulin and TGF-
131 β signaling, contributed to H_2S-evoked avoidance (***Supplementary file 1***). A naturally
132 occurring variant of the neuropeptide receptor gene *npr-1*, previously implicated in the
133 modulation of O_2 and CO_2 responses, also affected locomotory speed in H_2S (***Supplementary***
134 ***file 1***). In addition, mitochondrial components, including those involved in respiration and H_2S
135 detoxification, played critical roles in triggering and maintaining escape behavior in H_2S. In
136 contrast, we did not find evidence that globins, K^+ channels, or biogenic amine signaling
137 contributed significantly to the behavioral avoidance to H_2S (***Supplementary file 1***).
138

139 **cGMP signaling in ASJ cilia contributes to H_2S avoidance**

140 One group of mutants exhibiting reduced locomotory speed in H_2S had defects in ciliogenesis
141 (***Figure 2A–C***). This group included *daf-19* mutants lacking cilia, *dyf-3* mutants with reduced
142 cilia length, and *dyf-7* mutants in which ciliogenesis occurs but the cilia are not anchored to
143 their sensilla and are not exposed to the external environment (Heiman & Shaham, 2009;
144 Murayama, Toh, Ohshima, & Koga, 2005; Starich et al., 1995; Swoboda, Adler, & Thomas,
145 2000). These findings suggest that ciliogenesis and exposure of cilia to the external
146 environment are essential for animals to escape H_2S exposure. In addition, these mutants
147 exhibited consistently high reversal rate, likely associated with their reduced locomotory speed
148 (***Figure 2—figure supplement 1A–F***). Cilia-mediated sensory responses often involve the

activation of guanylate cyclases and the opening of cGMP-gated channels (Ferkey, Sengupta, & L'Etoile, 2021). We observed significantly attenuated locomotory speed in response to H_2S in *tax-4* or *tax-2* mutants, which lack key subunits of cilia-enriched cGMP-gated channels (***Figure 2D, E***). In a comprehensive survey of all guanylate cyclase mutants, the *daf-11* strain emerged as the only mutant showing speed response defects in the avoidance of H_2S (***Figure 2D, supplementary file 1***). Similar to the cilia mutants, animals deficient in *daf-11* had low speed, attenuated omega turns, and constantly high reversal rate (***Figure 2D, Figure 2—figure supplement 1G, H***). Selective expression of *daf-11* in ASJ neurons, but not in other neurons, partially restored the speed response to acute H_2S (***Figures 2F, Figure 2—figure supplement 2A–D***). In addition, the H_2S response defect of *tax-4* mutants was also rescued by selective expression of its cDNA in ASJ neurons (***Figure 2G***), suggesting that the receptor guanylate cyclase DAF-11 and the CNG channel TAX-4 act at least partially in ASJ neurons to promote acute avoidance to H_2S. To validate the role of ASJ neurons in H_2S responses, we blocked neurotransmission from ASJ using the catalytic domain of *Tetanus Toxin (TeTx*), which impairs neurosecretion by specifically cleaving synaptobrevin (Schiavo et al., 1992). Cell-specific expression of *TeTx* in ASJ significantly inhibited the speed response to H_2S ***(Figure 2H)***. Surprisingly, using the Ca^{2+} sensor GCaMP6s to monitor a direct response of ASJ neurons to H_2S, we observed no H_2S-induced Ca^{2+} transients under any of the tested conditions, whereas CO_2-evoked Ca^{2+} increases were readily detected ***(Figure 2I, Figure 2—figure supplement 2E).*** These findings suggest that although ASJ neuronal activity and neurosecretion contribute to the H_2S responses, ASJ neurons are unlikely to play a role in directly detecting H_2S.

Starvation modulates H_2S avoidance

In the candidate gene screen, another set of mutants with reduced speed responses to H_2S had previously been shown to be defective in response to CO_2 (Hallem & Sternberg, 2008). Specifically, the H_2S-evoked speed response was reduced in mutants deficient in nutrient-sensitive signaling, including the insulin receptor DAF-2, the TGF-β ligand DAF-7, and the nuclear hormone receptor NHR-49 (***Figure 3A–C, Figure 3—figure supplement 1A***).

177 Similarly, mutants lacking other CO_2 response modulators, such as the calcineurin subunits
178 TAX-6 and CNB-1, also failed to respond to H_2S (***Figure 3—figure supplement 1B, C***). In
179 addition to the abolished speed response, we also observed that the H_2S-evoked omega-turn
180 response was nearly abolished in *daf-2* mutants, and high proportion of animals exhibited
181 persistently high reversal rate regardless of H_2S stimulation (***Figure 3—figure supplement 1D–***
182 ***F***). The H_2S avoidance defects observed in *daf-2* and *daf-7* single mutants were fully
183 suppressed in *daf-2; daf-16* and *daf-7; daf-3* double mutants ***(Figure 3A, B).*** Therefore, it is
184 likely that insulin and TGF-β signaling modulate H_2S responses by regulating the expression
185 of relevant genes via DAF-16 and DAF-3 transcription factors, respectively. Given that H_2S-
186 evoked speed response was modulated by the nutrient-sensitive pathways, we further explored
187 whether the locomotory response to H_2S was sensitive to the nutrient state. Similar to the
188 response to CO_2 (Bretscher et al., 2008; Hallem & Sternberg, 2008), we observed that a 24-
189 hour period of starvation suppressed the speed response to H_2S ***(Figure 3D).*** However, the CO_2
190 sensor GCY-9 was dispensable for H_2S-evoked avoidance ***(Figure 3—figure supplement 1G–***
191 ***I).*** These findings suggest that while acute avoidance of CO_2 and H_2S share common
192 modulatory pathways, the responses are initiated through distinct mechanisms.
193
194 **The O_2 sensing circuit antagonizes H_2S avoidance in wild isolates**
195 Wild strains of *C. elegans* thrive in environmental niches characterized by variable O_2, CO_2
196 and H_2S levels (Adams et al., 1979; Bretscher et al., 2008; Budde & Roth, 2011; Gea, Barrena,
197 Artola, & Sanchez, 2004; Hallem & Sternberg, 2008; Morra & Dick, 1991; Oshins, Michel,
198 Louis, Richard, & Rynk, 2022; Patange et al., 2025; Rodriguez-Kabana et al., 1965). Compared
199 to the laboratory reference strain N2, wild isolates display robust responses to high O_2 but
200 reduced sensitivity to CO_2 stimulation (Beets et al., 2020; Bretscher et al., 2008; Carrillo,
201 Guillermin, Rengarajan, Okubo, & Hallem, 2013; Hallem & Sternberg, 2008; Kodama-Namba
202 et al., 2013; McGrath et al., 2009). It is thought that the unique O_2 and CO_2 responses of N2
203 strain evolved during its domestication on solid media at atmospheric gas concentrations
204 (Sterken, Snoek, Kammenga, & Andersen, 2015). We hypothesized that wild *C. elegans* strains

205 might also exhibit an attenuated response to H_2S, and therefore included a set of wild strains in
206 our candidate gene screen. Consistent with this hypothesis, wild isolates including CB4855,
207 CB4856, and CB4858 exhibited reduced locomotory speed in H_2S (***Figure 3E, Figure 3—***
208 ***figure supplement 1J***).

209 A naturally occurring variation in the neuropeptide receptor NPR-1 predominantly
210 determines the differences in locomotory responses to O_2 and CO_2 between the laboratory N2
211 strain and wild isolates. The NPR-1(215F) variant found in wild isolates is less active than the
212 NPR-1(215V) found in N2 animals (de Bono & Bargmann, 1998). We wondered whether the
213 variations in the *npr-1* gene also contribute to differences in the acute response to H_2S. The
214 absence of *npr-1* was sufficient to reduce the speed response to H_2S, suggesting that active
215 NPR-1 signaling promotes H_2S avoidance (***Figure 3F***). NPR-1(215V) primarily acts within the
216 RMG interneurons to modulate responses to environmental stimuli by inhibiting signal output
217 from these neurons (***Figure 3G***) (Laurent et al., 2015; Macosko et al., 2009). Cell-specific
218 expression of the highly active *npr-1(215V)* variant in RMG neurons effectively restored the
219 H_2S-evoked locomotory speed in *npr-1* null mutant worms (***Figure 3H***). Furthermore,
220 optogenetic stimulation of RMG interneurons using channelrhodopsin-2 (ChR2) significantly
221 dampened the locomotory response to H_2S in N2 animals, suggesting that high RMG activity
222 inhibits H_2S responses (***Figure 3—figure supplement 1K***).

223 The perception of 21% O_2 involves the soluble guanylate cyclases GCY-35/GCY-36
224 and the downstream cyclic nucleotide-gated (CNG) channels TAX-4/TAX-2 in the URX, AQR,
225 and PQR O_2-sensing neurons, which relay the signals to RMG (Busch et al., 2012; Cheung,
226 Cohen, Rogers, Albayram, & de Bono, 2005; Couto, Oda, Nikolaev, Soltesz, & de Bono, 2013;
227 Gray et al., 2004; Laurent et al., 2015; Persson et al., 2009; Zimmer et al., 2009). We
228 investigated whether disrupting the O_2 sensing machinery would have the same effect as
229 inhibiting RMG signaling pathway by NPR-1(215V). Mutating *gcy-35* and *tax-4*, or genetically
230 ablating the O_2 sensing neurons URX, AQR, and PQR by cell-specific expression of the pro-
231 apoptotic gene *egl-1* restored H_2S-evoked speed response in *npr-1* null mutants (***Figure 3I–K***).
232 Specific expression of *gcy-35* cDNA in O_2 sensing neurons was sufficient to repress this

233 response to H_2S in *npr-1; gcy-35* double mutants (***Figure 3L***). Finally, enhancing the
234 presynaptic activity of URX, AQR, PQR neurons by the expression of a gain-of-function PKC-
235 1(A160E) (Dekker, Mcintyre, & Parker, 1993; Hiroki et al., 2022) significantly dampened H_2S-
236 induced locomotory speed (***Figure 3—figure supplement 1L***). Taken together, these
237 observations indicate that activation of the O_2-sensing circuit inhibits the neural pathway
238 required for H_2S-evoked avoidance response.
239
240 **H_2S exposure reprograms gene expression in *C. elegans***
241 Wild isolates that were relatively insensitive to H_2S exposure (***Figure 3E, Figure 3—figure***
242 ***supplement 1J***) likely evolved adaptations to persist in environments where H_2S levels may
243 transiently increase (Budde & Roth, 2011; Patange et al., 2025; Rodriguez-Kabana et al., 1965;
244 Romanelli-Cedrez et al., 2024). These adaptations to H_2S are mediated, at least in part, by the
245 reprogramming of gene expression (Miller et al., 2011). To identify the genes whose expression
246 was induced by prolonged H_2S exposure, we conducted a comparative analysis of transcriptome
247 profiles in animals exposed to 50 ppm or 150 ppm H_2S for 1 hour, 2 hours, or 12 hours. RNA-
248 seq analysis revealed that exposure to either 50 ppm or 150 ppm H_2S for one hour was sufficient
249 to trigger significant changes in gene expression, with 518 or 304 genes showing differential
250 expression, respectively (***Figure 4A, Supplementary file 2***). Genes induced by H_2S exposure
251 for 1 or 2 hours displayed considerable overlap (***Figure 4B, Figure 4—figure supplement 1A***).
252 Gene Ontology (GO) analysis revealed that biological processes such as defense against
253 bacteria and cysteine biosynthesis from L-serine were significantly enriched after H_2S exposure
254 (***Figure 4C, D, Figure 4—figure supplement 1B, C***). As expected, we observed a robust
255 induction of genes involved in H_2S detoxification (***Figure 4E, F***) (Horsman & Miller, 2016;
256 Miller et al., 2011; Niu et al., 2011; Vora et al., 2022). H_2S is detoxified in mitochondria by
257 sulfide:quinone oxidoreductase SQRD-1 to produce persulfide, which is then metabolized by
258 sulfur dioxygenase ETHE-1 to generate sulfite. Thiosulfate transferase further oxidizes sulfite
259 to produce thiosulfate (Hildebrandt & Grieshaber, 2008). Glutathione S-transferases (GSTs)
260 remove accumulated sulfur molecules during H_2S oxidation (Jackson, Melideo, & Jorns, 2012).

261 Notably, *gst-19* and *sqrd-1* were among the most significantly upregulated genes after one or
262 two hours of exposure to either 50 ppm or 150 ppm H_2S, while *ethe-1* showed a weak increase
263 (***Figure 4E, F, Figure 4—figure supplement 1D, E, Supplementary file 2***).

264 H_2S exposure is known to activate the HIF-1 pathway (Budde & Roth, 2010, 2011;
265 Horsman et al., 2019; Ma et al., 2012; Miller et al., 2011; Powell-Coffman, 2010; Topalidou &
266 Miller, 2017). In line with this, a proportion of genes with HIF-1 regulated promoters displayed
267 increased expression after 1 or 2 hours of H_2S exposure (***Figure 4—figure supplement 1F***).
268 Among these were the aforementioned detoxifying enzymes GST-19, SQRD-1, and ETHE-1,
269 as well as CYSL-1, CYSL-2, and CDO-1, which are involved in cysteine metabolism
270 (***Supplementary file 2***). Consistent with earlier studies, we also observed differential expression
271 of a set of SKN-1 targets in response to chronic H_2S exposure (***Figure 4—figure supplement***
272 ***1G***) (Horsman et al., 2019; Miller et al., 2011; Niu et al., 2011). This included the heat shock
273 protein genes *hsp-16.2* and *hsp-16.41* (***Figure 4E, F, Figure 4—figure supplement 1D, E***).
274 Surprisingly, we detected a rapid increase in the expression of genes associated with
275 intracellular H_2S production, including the methanethiol oxidase-encoding gene *semo-1* and the
276 mercaptopyruvate sulfurtransferase-encoding gene *mpst-3* (***Figure 4E, F, Figure 4—figure***
277 ***supplement 1D, E***) (Philipp et al., 2022; Qabazard et al., 2014). Elevated expression of 3-
278 mercaptopyruvate sulfurtransferase has similarly been reported in sulfide spring fish,
279 suggesting a conserved response mechanism to H_2S (Kelley et al., 2016; Mathew, Schlipalius,
280 & Ebert, 2011; Qabazard et al., 2014). However, the functional implications of increased
281 expression of H_2S synthesis genes remains unclear.

282 When exposed to H_2S for 12 hours, the differentially expressed genes showed reduced
283 overlap with those identified at earlier time points (***Figure 4B, Figure 4—figure supplement***
284 ***1A***), suggesting that distinct defense strategies may be employed at various stages of H_2S
285 exposure. Furthermore, substantial overlap was observed between the sets of genes induced by
286 50 ppm and 150 ppm H_2S after 1h or 2h exposure. However, this overlap decreased
287 significantly after 12 hours exposure (***Figure 4—figure supplement 1H–J***). Additionally, we
288 noticed that 150 ppm H_2S specifically triggered the expression of the HIF-1 regulator *rhy-1* and

289 the HIF-1 target *nhr-57* at all exposure time points, a response that was less pronounced at 50
290 ppm H_2S (***Figures 4E, F, Figure 4—figure supplement 1D, E, K and L***). Together, these
291 findings suggest that multiple defense mechanisms are induced to adapt to the stress imposed
292 by H_2S, which can diverge over time and at different H_2S concentrations.
293
294 **Locomotory speed response to H_2S is modulated by HIF-1-induced detoxification**
295 Given that HIF-1 signaling is robustly activated shortly after H_2S exposure (***Figure 4—figure***
296 ***supplement 1F***) (Budde & Roth, 2010, 2011; Miller et al., 2011), we next sought to determine
297 how HIF-1 signaling might contribute to H_2S-evoked avoidance response, and began by
298 examining the effects of HIF-1 stabilization. Acclimating animals in 1% O_2 for 12 hours or
299 longer significantly decreased the speed response to H_2S, indicating that HIF-1 stabilization
300 inhibits the H_2S-evoked avoidance behavior **(*Figure 5A*)**. To confirm this observation, we
301 examined several mutants with stabilized HIF-1. The conserved proline-4-hydroxylase
302 PHD/EGL-9 and the von Hippel-Lindau (VHL) tumor suppressor protein are required for HIF-
303 1 degradation (Kaelin & Ratcliffe, 2008; Semenza, 2010). Disruption of either *egl-9* or *vhl-1*
304 leads to HIF-1 stabilization under normoxic conditions. Similar to the effect of prolonged
305 hypoxia, both mutants exhibited a markedly reduced locomotory speed in H_2S **(*Figure 5B*).**
306 Interestingly, the omega-turn and reversal responses to H_2S were also substantially inhibited in
307 *egl-9* mutants **(*Figure 5—figure supplement 1A, B*)**. In contrast, the locomotory speed
308 response to 1% O_2 remained largely unaffected in *egl-9* deficient animals **(*Figure 5—figure***
309 ***supplement 1C*),** suggesting a selective impairment of the H_2S response. In addition, expressing
310 the non-degradable forms of HIF-1, *hif-1*(P621A or P621G), under the pan-neuronal *unc-14*
311 promoter or under the endogenous *hif-1* promoter, was sufficient to inhibit H_2S evoked speed
312 responses (***Figure 5C***). Together, these findings indicate that the activation of HIF-1 signaling
313 during prolonged H_2S or hypoxia exposure mediates an adaptive response associated with
314 reduced behavioral responses to H_2S, and that HIF-1 stabilization in neurons alone is sufficient
315 to promote this behavioral adaptation.

316 On the other hand, animals lacking HIF-1 signaling have previously been shown to
317 display increased sensitivity to H_2S and become paralyzed rapidly upon exposure (Budde &
318 Roth, 2010; Horsman et al., 2019). Consistent with this, *hif-1* mutants exhibited a brief increase
319 in speed upon H_2S exposure, which rapidly declined to baseline levels (***Figure 5D***). They also
320 displayed a stronger initial omega-turn response and greater inhibition of the reversal rate than
321 WT (***Figure 5E, F***), confirming that animals deficient in HIF-1 signaling are sensitized to H_2S
322 exposure. This transient avoidance behavior was also observed in *egl-9; hif-1* and *vhl-1; hif-1*
323 double mutants (***Figure 5G, H***), suggesting that this phenotype is linked to the absence of HIF-
324 1 signaling. Importantly, *hif-1* mutants displayed a robust speed response to other stimuli, such
325 as near-UV light and 1% O_2 stimulation ***(Figure 5I, Figure5—figure supplement 1D)***,
326 suggesting that the brief avoidance response is specific to H_2S rather than reflecting a general
327 locomotory defect. Further supporting increased sensitivity to H_2S in *hif-1* mutants, the
328 locomotory speed response of *hif-1* mutants to subsequent near-UV light stimulation was nearly
329 abolished after 30 minutes of H_2S exposure, whereas *egl-9* mutants and WT animals remained
330 fully responsive ***(Figure 5I)***. The reduced movement and lack of responsiveness to other
331 stressors in *hif-1* mutants resemble the stress-induced sleep-like behavior previously observed
332 in response to noxious heat (Byrne Rodgers & Ryu, 2020). Prompted by this observation, we
333 next explored whether HIF-1-induced detoxification genes were also required to maintain H_2S-
334 evoked behavioral responses (***Figure 5—figure supplement 1E)***. Similar to *hif-1* mutants,
335 *sqrd-1* and *ethe-1* mutants displayed brief responses to H_2S, with locomotory activity rapidly
336 returning to baseline levels ***(Figure 5J, K, Figure 5—figure supplement 1F–I)***. However, both
337 mutants responded normally to 1% O_2, suggesting a specific hypersensitivity to H_2S toxicity
338 ***(Figure 5—figure supplement 1J).*** Furthermore, we examined the contribution of additional
339 genes whose expression was upregulated in response to H_2S, including the
340 sulfhydrylase/cysteine synthase-encoding genes *cysl-1*, *cysl-2*, and *cysl-3*, as well as *semo-1*.
341 Disrupting any of these genes phenocopied the responses observed in *hif-1, ethe-1*, or *sqrd-1*
342 mutants, while they displayed normal responses to 1% O_2 (***Figure 5L, Figure 5—figure***
343 ***supplement 1D, K–P***). These observations suggest that while the HIF-1-induced H_2S

344 detoxification system is not essential for initiating the response to H_2S, it is required to maintain
345 animals' locomotory activity in the presence of H_2S.
346
347 **Labile iron pool sustains the locomotory activity in H_2S**
348 Among the most differentially regulated genes upon exposure to H_2S, we observed consistent
349 downregulation of *ftn-1* and to a lesser extent *ftn-2*, whereas *smf-3* expression was increased
350 under specific H_2S conditions (***Figure 6A, B, Figure 6—figure supplement 1A–D***). The
351 ferritin-encoding genes *ftn-1* and *ftn-2,* along with the iron transporter *smf-3*, are critical for
352 maintaining intracellular labile iron homeostasis in *C. elegans* (Ackerman & Gems, 2012;
353 Gourley, Parker, Jones, Zumbrennen, & Leibold, 2003; Rajan et al., 2019; Romney, Newman,
354 Thacker, & Leibold, 2011), suggesting that H_2S exposure may interfere with cellular iron
355 storage. It has been shown that disrupting *ftn-1* increases labile iron pools in the cytoplasm,
356 while its overexpression reduces these levels (Anderson & Leibold, 2014; Romney et al., 2011).
357 We found that *ftn-1* mutants had enhanced speed response to H_2S, whereas *ftn-1* overexpression
358 attenuated H_2S-induced speed increase without damaging acute response to 1% O_2 (***Figure 6C,***
359 ***D, Figure 6—figure supplement 1E)***. In addition, *smf-3* mutants, which impair iron uptake,
360 exhibited a reduced speed response to H_2S (***Figure 6D***). These results support the idea that H_2S
361 exposure disrupts iron homeostasis.
362 To complement our genetic analysis, we pharmacologically depleted labile irons. In
363 the presence of the iron chelator 2,2'-dipyridyl (BP), the H_2S-evoked speed response was fully
364 lost (***Figure 6E***), whereas locomotory speed in response to hypoxia was maintained (***Figure***
365 ***6—figure supplement 1F).*** We noticed that, similar to *hif-1* mutants, both *smf-3* mutants and
366 BP-treated animals exhibited a strong initial omega-turn response to H_2S (***Figure 6—figure***
367 ***supplement 1G, I)***, suggesting that these animals are hypersensitive to H_2S toxicity. One
368 possibility is that low iron levels compromise H_2S detoxification capacity, as the detoxification
369 enzyme ETHE-1 requires iron for its activity (Kabil & Banerjee, 2012; Pettinati, Brem,
370 McDonough, & Schofield, 2015). By contrast, increasing iron levels by feeding ferric
371 ammonium citrate (FAC) or by disrupting *ftn-1* significantly sustained animals' locomotory

372 speed in H_2S (***Figure 6D, E***), likely by delaying H_2S-mediated iron depletion. However, the
373 reorientation and reversals were not significantly affected (***Figure 6—figure supplement 1G–***
374 ***J***). This impact of FAC supplementation and *ftn-1* disruption on speed response was largely
375 lost in the absence of *hif-1* (***Figure 6F, G***), suggesting that the effects of iron require HIF-1-
376 dependent detoxification (***Figure 6H)***. Yet, increased iron availability modestly improved the
377 locomotory activity of *hif-1* mutants in H_2S (***Figure 6F, G***), presumably by compensating for
378 the low iron levels in *hif-1* mutant animals (Rajan et al., 2019; Romney et al., 2011).
379
380 **Mitochondrial function modulates H_2S-evoked locomotion responses**
381 The mitochondrial electron transport chain (ETC) is not only the primary target of H_2S
382 toxicity, but is also an essential component of the H_2S detoxification pathways (Cooper &
383 Brown, 2008; Khan et al., 1990; Nicholls & Kim, 1982; Romanelli-Cedrez et al., 2024).
384 Based on this, we hypothesized that ETC plays a central role in the locomotory response to
385 H_2S. Indeed, mutating the genes critical for ETC function, including *gas-1*, *clk-1*, *mev-1,* and
386 *isp-1*, impaired the H_2S-evocked speed and reversal responses (***Figure 7A–D, Figure 7—***
387 ***figure supplement 1A–D)***. These data suggest either that dysfunctional ETC induces an
388 adaptive response to cellular stressors or that a functional ETC is required to trigger and
389 support H_2S-evoked avoidance behavior. Consistent with the later model, exposing animals to
390 rotenone, an ETC complex I inhibitor, robustly inhibited the speed responses to H_2S at all
391 time points we tested (***Figure 7E***). Similar to ETC mutants, WT animals exposed to rotenone
392 for 2 hours also showed reduced basal locomotory activity (***Figure 7E***).
393 In contrast to prolonged rotenone exposure, we noticed that transient rotenone
394 exposure substantially increased animals' basal locomotory speed (***Figure 7E***) (Onukwufor et
395 al., 2022), suggesting that acute ETC interruption evokes behavioral avoidance, in a manner
396 similar to that observed with other noxious stimuli. Since rotenone rapidly and persistently
397 stimulates mitochondrial ROS production (Ochi et al., 2016; Ramsay & Singer, 1992; Zorov,
398 Juhaszova, & Sollott, 2014), the transient locomotory increase during short rotenone exposure
399 (***Figure 7E***) is likely driven by these ROS bursts, whereas reduced locomotory activity during

400 prolonged exposure is presumably caused by chronically elevated ROS production. As toxic
401 levels of H_2S also induce ROS (Jia et al., 2020), this raised the possibility that H_2S-evoked
402 behavioral responses were modulated by the mitochondrial ROS. Therefore, we sought to
403 further explore how mitochondrial ROS contributes to speed response to high H_2S. We
404 focused on superoxide dismutases (SODs), key enzymes in superoxide detoxification. The *C.*
405 *elegans* genome encodes five *sod* genes: *sod-1* and *sod-5* encode cytosolic Cu/ZnSODs, *sod-2*
406 and *sod-3* encode mitochondrial MnSODs, and *sod-4* encodes the extracellular Cu/ZnSOD
407 isoforms (Doonan et al., 2008; Zubovych, Straud, & Roth, 2010). All *sod* single mutants
408 exhibited a robust initial response to 150 ppm H_2S ***(Figure 7F, G).*** Interestingly, the
409 mitochondrial SOD mutants *sod-2* and *sod-3*, as well as *sod-5*, showed an initial burst of
410 locomotory activity followed by a rapid decline in speed in the presence of H_2S ***(Figure 7F,***
411 ***G)***, but maintained a high locomotory speed in response to 1% O_2 ***(Figure 7—figure***
412 ***supplement 1E)***. In the quintuple *sod-1; sod-2; sod-3; sod-4; sod-5* mutant, which lacks all
413 superoxide dismutases and presumably accumulates higher ROS levels, the H_2S-evoked speed
414 and omega-turn responses were nearly abolished, and the proportion of animals exhibiting
415 reversals remained consistently high, a pattern resembling that of *egl-9* and ETC mutants
416 ***(Figure 7G, Figure 7—figure supplement 1F, G)***. Similar to *sod-2* and *sod-3*, the quintuple
417 *sod* mutant exhibited robust speed response to 1% O_2 (Zhao et al., 2022). In addition, the
418 quintuple mutants responded normally to near-UV light after 30 minutes of H_2S exposure
419 (***Figure 7—figure supplement 1H)***, indicating that their neuromuscular function remains
420 largely preserved. These observations suggest that either constitutively high ROS levels in
421 quintuple mutants dampen H_2S-evoked ROS transients, or they promote adaptation to H_2S-
422 induced stress, presumably via activation of stress-responsive pathways such as HIF-1,
423 NRF2/SKN-1, and DAF-16/FOXO, ultimately reducing the locomotory responses (***Figure***
424 ***7H***) (Lee, Hwang, & Kenyon, 2010; Lennicke & Cocheme, 2021; Patten, Germain, Kelly, &
425 Slack, 2010).
426
427 **Discussion**

428 Animals' behavior and physiology are profoundly influenced by the environments in which
429 they evolved. The laboratory strain N2, which is adapted to low atmospheric CO_2 and H_2S
430 concentrations, robustly avoids both gases (Beets et al., 2020; Bretscher et al., 2008; Carrillo
431 et al., 2013; Hallem & Sternberg, 2008; Kodama-Namba et al., 2013; McGrath et al., 2009).
432 Upon acute exposure to H_2S above 75 ppm, N2 exhibits an avoidance behavior characterized
433 by reorientation and increased locomotion. This response is significantly reduced in wild
434 isolates. These divergent responses between the laboratory strain and wild isolates are primarily
435 driven by variations in the *npr-1* gene, which encodes a neuropeptide receptor, suggesting that
436 *C. elegans* has undergone rapid evolutionary adaptation to its environment.

437 The behavioral response to a specific sensory stimulus is usually shaped by an interplay
438 of multiple environmental and physiological cues. We observe that conditions dampening *C.*
439 *elegans'* response to CO_2 also impair the response to H_2S. Specifically, the speed response to
440 H_2S is significantly inhibited at high O_2 levels, and in mutants with defective insulin or TGF-β
441 pathway that signal starvation. However, despite these shared modulations, CO_2 and H_2S
442 responses involve distinct molecular mechanisms. For example, CO_2 responses are mediated
443 by the guanylate cyclase GCY-9 in BAG neurons (Hallem et al., 2011), which is dispensable
444 for H_2S responses. In addition, acute exposure to H_2S induces a delayed acceleration compared
445 to CO_2. These data suggest that while responses to the two gases share a downstream neural
446 circuit that can be dynamically modulated by the state of O_2 sensing circuit, they are triggered
447 by distinct mechanisms.

448 In a candidate gene survey, we excluded the potential involvement of globins, K^+
449 channels, biogenic amines, and most guanylate cyclases in H_2S responses. However, we
450 observed that H_2S avoidance requires the activity of guanylate cyclase DAF-11 in ASJ neurons,
451 as well as neurosecretion from these neurons. Since the DAF-11 pathway and neurosecretion
452 from ASJ neurons regulate developmental programs that modify sensory functions in *C.*
453 *elegans* (Murakami, Koga, & Ohshima, 2001), it is not surprising that *daf-11* mutants display
454 pleiotropic phenotypes including impaired H_2S and CO_2 responses (Hallem & Sternberg, 2008).
455 In addition, we did not detect an H_2S-evoked calcium transient in ASJ neurons. Therefore,

456 although ASJ neurons and DAF-11 activity are clearly required, how H_2S avoidance is triggered
457 remains to be elucidated.

458 Consistent with previous reports (Horsman et al., 2019; Miller et al., 2011), H_2S
459 exposure substantially alters the gene expression in *C. elegans*, including those involved in H_2S
460 detoxification and iron homeostasis pathways. The repression of *ftn-1* and induction of *smf-3*
461 observed during H_2S exposure suggest that H_2S depletes intracellular labile iron. Iron is a
462 critical cofactor required for the activity of many enzymes and supports a wide range of cellular
463 processes (Dev & Babitt, 2017; Hentze, Muckenthaler, & Andrews, 2004). One important
464 enzyme that requires labile iron as cofactor is PHD/EGL-9, which targets HIF-1 for degradation.
465 Changes in iron availability are therefore expected to modulate EGL-9 activity, which in turn
466 alter the expression of HIF-1-regulated genes (Liochev, 1996; Myllyharju & Kivirikko, 1997;
467 Read, Bentley, Archer, & Dunham-Snary, 2021; Xu & Moller, 2011). However, ETHE-1, a
468 key H_2S detoxification enzyme upregulated upon HIF-1 stabilization, also requires iron for its
469 persulfide dioxygenase activity (Kabil & Banerjee, 2012; Pettinati et al., 2015). Therefore, H_2S-
470 evoked responses under varying iron availability are determined by the combined effects of
471 labile iron on HIF-1 signaling and on the H_2S detoxification enzymes, among other factors. For
472 instance, although reduced iron availability in *smf-3* or BP-treated animals may promote the
473 HIF-1 induced detoxification pathways by inactivating EGL-9, the actual enzymatic clearance
474 of H_2S is impaired due to low ETHE-1 activity. Supporting this, *smf-3* mutants and BP-treated
475 animals display increased sensitivity to H_2S, including enhanced initial omega-turn responses
476 and rapid inhibition of locomotion. In contrast, increased iron availability in *ftn-1* mutants or
477 FAC-treated animals likely delays iron depletion during H_2S exposure, preserving ETHE-1
478 detoxification capacity and postponing the onset of HIF-1-mediated adaptations that are
479 associated with reduced locomotion. This may explain the sustained high locomotory speed
480 observed in *ftn-1* mutants or FAC-treated animals. In the absence of HIF-1, iron
481 supplementation only partially improves the locomotory response to H_2S, likely because the
482 H_2S detoxification system including ETHE-1 cannot be transcriptionally induced. The modest
483 effect observed may instead reflect correction of iron deficiency in *hif-1* mutants.

484 At concentrations below 50 ppm, H_2S is well tolerated or even preferred, with
485 beneficial effects such as improved thermotolerance (Fawcett et al., 2015; Miller & Roth, 2007;
486 Qabazard et al., 2014). Notably, behavioral avoidance is absent below 50 ppm H_2S, suggesting
487 that escape behavior is triggered only when H_2S is not efficiently detoxified. This led us to
488 hypothesize that animals with enhanced detoxification capacity would show reduced avoidance
489 of otherwise toxic H_2S levels. Indeed, the speed response to H_2S is attenuated when the
490 detoxification program is upregulated under conditions of constitutive activation of HIF-1, such
491 as in *egl-9* or *vhl-1* mutants, after prolonged exposure to 1% O_2, or when HIF-1 signaling is
492 specifically activated in neurons. These observations support the idea that the initial avoidance
493 response to H_2S is triggered by neuronal detection of acute toxicity, while the subsequent
494 decline in speed reflects a rapid activation of adaptive mechanisms, particularly through
495 stabilization of HIF-1. The fact that wild type animals remain responsive to other stimuli after
496 prolonged H_2S exposure suggests that reduced locomotory speed in H_2S reflects active
497 desensitization rather than general paralysis. However, persistently high H_2S exposure is likely
498 to exhaust cellular defense systems, leading to toxicity and paralysis. By contrast, the rapid loss
499 of locomotion observed in *hif-1* mutants and detoxification-defective mutants is mediated by a
500 mechanism distinct from adaptation. Their loss of responsiveness to other stimuli after H_2S
501 exposure suggests that these animals likely become sensitized and rapidly intoxicated by H_2S
502 due to impaired detoxification. Therefore, H_2S exposure promotes a behavioral program that
503 includes an initial reorientation and acceleration responses followed by a progressive adaptation
504 driven by cellular detoxification processes. A similar behavioral program has been observed in
505 *C. elegans* during noxious heat exposure, which induces short-term heat avoidance followed
506 by long-lasting cytoprotective adaptation and a gradual reduction in avoidance (Byrne Rodgers
507 & Ryu, 2020).

508 The interaction of H_2S with mitochondrial ETC is multifaceted, acting as an electron
509 donor at low concentrations and becoming a potent toxicant at high levels (Szabo et al.,
510 2014), in part by promoting superoxide generation through complex IV inhibition and reverse
511 electron transport at complex I (Cooper & Brown, 2008; Jia et al., 2020; Khan et al., 1990;

512 Nicholls & Kim, 1982; Romanelli-Cedrez et al., 2024). We propose that mitochondria play a
513 dual role in H_2S-evoked locomotory avoidance. On one hand, the mitochondrial ETC
514 contributes to H_2S detoxification and promotes adaptation. On the other hand, toxic levels of
515 H_2S remodel the ETC, leading to increased ROS production, which may serve as a trigger for
516 the avoidance response. Supporting the idea that acute mitochondrial ROS generation initiates
517 avoidance of high H_2S levels, short-term rotenone exposure, known to promote mitochondrial
518 ROS formation (Ochi et al., 2016; Ramsay & Singer, 1992; Zorov et al., 2014), substantially
519 increases locomotory speed (Onukwufor et al., 2022). Meanwhile, the speed response to high
520 H_2S is fully suppressed by rotenone. This inhibition could result either from excessive
521 mitochondrial ROS generated by rotenone, which may dampen the H_2S-triggered ROS spike,
522 or from direct complex I inhibition, which may disrupt other H_2S signaling processes required
523 to initiate avoidance. However, persistent mitochondrial ROS production appears to suppress
524 high locomotory speed and inhibit responsiveness to H_2S, as observed after 2-hour rotenone
525 exposure, in mitochondrial ETC mutants, and in animals lacking all superoxide dismutases.
526 One likely explanation is that mitochondrial ROS can activate a variety of stress-responsive
527 pathways, including HIF-1, NRF2/SKN-1, and DAF-16/ FOXO signaling (Lee et al., 2010;
528 Lennicke & Cocheme, 2021; Patten et al., 2010), priming animals' adaptation to prolonged
529 stress rather than causing toxicity. This is supported by the observation that even though
530 SOD-deficient animals do not display strong initial locomotory responses to H_2S, they remain
531 responsive to other stimuli after 30 minutes of H_2S exposure, suggesting that high ROS levels
532 do not compromise general viability or the H_2S detoxification capacity. Therefore, we favor a
533 model in which mitochondrial ROS exert a biphasic effect on H_2S-induced avoidance,
534 facilitating H_2S avoidance under acute conditions, and contributing to locomotory inhibition
535 when it is chronically elevated. Overall, lack of a clear sensory machinery, the slow increase
536 of locomotory speed in H_2S (***Figure 1D***), the rotenone-evoked speed responses, and the
537 strong modulation of H_2S responses by mitochondrial ETC inhibition suggest that H_2S may
538 not be directly perceived by *C. elegans*. Instead, acute avoidance to H_2S is likely initiated by
539 ROS-induced toxicity.

540 In summary, this study unveils a novel behavior of *C. elegans* in their avoidance to
541 H_2S. The speed response to H_2S is intricately shaped by environmental context, integrating
542 inputs from other sensory cues such as food availability and O_2 levels. Our findings suggest
543 that H_2S-induced locomotion arises from acute remodeling of mitochondrial ETC and
544 associated ROS production, while highlighting the vital role of the HIF-1-induced
545 detoxification pathways and iron homeostasis in protecting against H_2S-induced mitochondrial
546 toxicity. Further work is needed to validate this model and to elucidate the neural circuits
547 mediating the behavioral response to ROS-induced toxicity.
548

549 **Materials and Methods**

550 **Strains**

551 *C. elegans* were maintained using standard protocols (Brenner, 1974). Strains used in this study
552 are listed in ***Supplementary file 1*** and ***Supplementary file 3***.
553

554 **Preparation of H_2S gas mixture**

555 Different H_2S concentrations were created as previously described (Miller & Roth, 2007).
556 Briefly, the H_2S-containing gas mixture were prepared by diluting 5000 ppm H_2S in nitrogen
557 (N_2) with 7% O_2 balanced with N_2. The gas flow was tuned by Sierra Smart-Trak 100 mass
558 flow controllers. H_2S concentration in the mixture was measured using two H_2S detectors (MSA
559 ALTAIR 2X gas detector for H_2S and Clip Single Gas Detector, SDG, CROWCON). The pre-
560 defined gas mixtures of 7% O_2, 1% O_2 and 5% CO_2 with N_2 were purchased from Air Liquide
561 Gas AB. 5000 ppm H_2S stock in N_2 was obtained from Linde Gas AB. Gas mixtures in all
562 experiments were hydrated before use.
563

564 **Molecular Biology**

565 The Multisite Gateway system (Thermo Fisher Scientific, United States) was used to generate
566 expression vectors. Promoters, including *gcy-37* (2.7kb), *trx-1* (1 kb), *ftn-1*(2 kb), *daf-11*(3 kb),
567 *odr-3*(2.7 kb), *gpa-11*(3 kb), *sra-6*(3 kb), *odr-1*(2.4 kb), *flp-21*(4.1kb), and *ocr-2*(2.4 kb) were

568 amplified from N2 genomic DNA and cloned into pDONR P4P1 using BP clonase. g*cy-35*,
569 *tax-4,* and *pkc-1* cDNAs were amplified using the first strand cDNA library as the template,
570 while *daf-11* and *ftn-1* genomic sequences were amplified using genomic DNA as the template.
571 The entry clones of these genes pDONR 221 were generated using BP reaction. To generate
572 the gain of function mutation of *pkc-1* (A160E), Q5 Site-Directed Mutagenesis Kit (NEB) was
573 used according to manufacturer instructions. All expression vectors were generated using LR
574 reaction. The primer sequences were displayed in ***Supplementary file 4***.
575 To generate transgenic animals, the *daf-11* expression vectors were injected at the
576 concentration of 20 ng/µl supplemented with 50 ng/µl of a coelomocyte co-injection marker
577 (*unc-122p::GFP)* and 30 ng/µl of 1kb DNA ladder. For *tax-4* gene, the injection mixtures were
578 prepared using 40 ng/µl of *tax-4* expression vectors, 50 ng/µl of a coelomocyte co-injection
579 marker and 10 ng/µl of 1kb DNA ladder. The rest of expression constructs were injected at 50
580 ng/µl together with 50 ng/µl of a coelomocyte marker.
581
582 **CRISPR/Cas9 genome editing**
583 Genes were disrupted using CRISPR/Cas9 mediated genome editing as described (Dokshin,
584 Ghanta, Piscopo, & Mello, 2018; Ghanta & Mello, 2020). The strategy involved the utilization
585 of homology-directed insertion of custom designed single strand DNA template (ssODN),
586 which had two homology arms of 35bp flanking the targeted PAM site. Between two homology
587 arms, a short sequence containing a unique restriction enzyme cutting site as well as in-frame
588 and out-of-frame stop codons, was included. The insertion of ssODN template would delete 16
589 bases of coding sequence, ensuring the proper gene disruption. To prepare the injection cocktail,
590 0.5 µl of Cas9 protein (IDT) was mixed with 5 µl of 0.4µg/µl tracrRNA (IDT, United States)
591 and 2.8 µl of 0.4 µg/µl crRNA (IDT). The mixture was incubated at 37°C for at least 10 minutes
592 before 2.2 µl of 1µg/µl ssODN (or 500 ng dsDNA) and 2 µl of 0.6 µg/µl *rol-6* co-injection
593 marker were added. Nuclease-free water was used to bring the final volume to 20 µl. The
594 injection mixture was centrifuged for 2 minutes before use.
595

596 **Behavioral assays**

597 H_2S evoked locomotion activity was monitored as described previously (Laurent et al., 2015;
598 Zhao et al., 2022). Briefly, OP50 bacteria were seeded on the assay plates 16 hours before use.
599 The border of bacterial lawn was removed using a PDMS stamp. For each assay, 25 to 30 day-
600 one adult animals were picked onto assay plates, allowed to settle down for 15 minutes, and
601 subsequently sealed within microfluidic chambers. A syringe pump (PHD 2000, Harvard
602 Apparatus) was employed to deliver gas mixtures into the microfluidic chamber at a constant
603 flow of 3 ml/min. The rapid switch between different gas mixtures were controlled by Telfon
604 valves coupled with ValveBank Perfusion Controller (AutoMate Scientific). The locomotory
605 activity at different gas mixtures were monitored using a high-resolution camera (FLIR)
606 mounted on a Zeiss Stemi 508 microscope. Videos were captured at a rate of 2 frames per
607 second, starting with a 2-minute recording in 7% O_2, followed by 10 or 11 minutes in H_2S, and
608 ending with 7% O_2. For the long-term recording in H_2S, video capture commenced with a 2-
609 minute period in 7% O_2, followed by a duration of 148 minutes in 150 ppm H_2S, and concluded
610 with a final 2-minute interval in 7% O_2. For each strain or condition, 3 to 4 replicates were
611 performed.

612 Near-UV light experiments were conducted to assess whether animals remained
613 responsive following a 30-minute incubation in 150 ppm H_2S balanced with 7% O_2. For each
614 experiment, 6-minute videos were recorded. The first 2 minutes captured the baseline
615 locomotion of the animals under white light, followed by 2 minutes of exposure to near-UV
616 light (435 nm, 0.7 mW/mm^2), and concluded with 2 minutes of white light. 3 to 4 replicates
617 were performed, with approximately 15 animals recorded per replicate.

618 The H_2S gradient experiment was performed in a PDMS chamber connected to a pump
619 delivering gas at 0.5 ml/min. To establish a gradient ranging from 150 ppm to 0 ppm H_2S, we
620 pumped 150 ppm H_2S balanced with 7% O_2 into one side and 7% O_2 into the opposite side.
621 After 25 minutes, the number of animals in each of the 5 sections was counted (***Figure 1G***).
622 Four replicates were performed, each using 30 day-one adult animals.

623 To assess the effects of rotenone on H_2S evoked locomotory response, day-one adult
624 animals were subjected to 10 μM rotenone for 10min, 30min, 1 hour and 2 hours on the drug
625 containing plates. Subsequently, the rotenone-treated animals were assayed on the standard
626 assay plates without the drug. To explore the impact of ferric ammonium citrate (FAC) (F5879,
627 Sigma-Aldrich) and 2,2′-Bipyridyl (BP) (D216305, Sigma-Aldrich) on behavioral response to
628 H_2S, L4 animals were exposed to 100 μM FAC or 5 mg/ml BP for 16 hours in the presence of
629 bacterial food. The FAC or BP treated animals were assayed on FAC or BP containing plates,
630 respectively.

631 Optogenetic experiments were performed as previously outlined (Zhao et al., 2022).
632 Transgenic L4 animals were exposed to 100 μM all-trans retinal (ATR) (R2500, Sigma) in the
633 dark for 16 hours. The ATR-fed animals were assayed under continuous illumination of 70
634 $\mu W/mm^2$ blue light, which was switched on at the start of recording at 7% O_2. Blue light was
635 emitted from an ultra-high-power LED lamp (UHP-MIC-LED-460, Prizmatix), and the light
636 intensity was determined using a PM50 Optical Power Meter (ThorLabs). To minimize the
637 effect of transmitted light on the transgenic animals, a long-pass optical filter was used to
638 eliminate the lights with short wavelengths during picking. All videos of behavioral analysis
639 were analyzed using a home-made MATLAB program Zentracker
640 (https://github.com/wormtracker/zentracker). For all behavior analyses, at least three assays
641 were performed for each strain with more than 80 worms in total.

642

643 **Ca^{2+} Imaging**

644 L4 animals expressing the GCaMP6s sensor in ASJ neurons were picked 24 hours before
645 imaging. The agarose pads were prepared 1 hour before the experiment. Animals were
646 incubated in 15 μl of 10 mM levamisole for 40 minutes prior to imaging. Between 15 and 20
647 animals were immobilized using 10 mM levamisole diluted in a concentrated OP50 bacterial
648 suspension and mounted on a 2% agarose pad in M9 buffer on a glass slide. The animals were
649 then covered with a microfluidic chamber. Imaging lasted for 16 minutes. O_2 (7%) was pumped

650 into the microfluidic chamber during the first and last 4 minutes. From minute 4 to 12, a mixture
651 of 7% O_2 and 150 ppm H_2S was pumped.
652 Imaging was performed on a Nikon AZ100 microscope equipped with a TwinCam
653 adapter (Cairn Research, UK), fitted with two DMK 33U monochrome cameras (The Imaging
654 Source, Germany). A 2x AZ Plan Fluor objective with 1x zoom was used, with an exposure
655 time of 300 ms. Excitation of GCaMP and RFP was provided by a CoolLED pE-300 (CoolLED,
656 UK). The TwinCam adapter was mounted with emission filters for green fluorescent protein
657 (510/20 nm) and red fluorescent protein (590/35 nm), along with a DC/T510LPXRXTUf2
658 dichroic mirror. Imaging data were analyzed using Neuron Analyzer, a custom-written Matlab
659 program for processing image stacks (code available at
660 https://github.com/neuronanalyser/neuronanalyser).
661
662 **RNA extraction and sequencing**
663 To obtain RNA samples for RNA-seq, thirty young adult animals were picked to each fresh
664 plate and allowed to lay eggs for 2 hours, after which the adult animals were removed and eggs
665 were allowed to develop into day-one adults. Day-one animals were subsequently challenged
666 with H_2S for three different time periods (1 hour, 2 hours and 12 hours). For each time period,
667 five plates of day-one animals were exposed to 50 ppm H_2S, 150 ppm H_2S or 7% O_2 as a control
668 group. Subsequently, the animals were immediately collected and rinsed three times with M9
669 buffer. After washing, the worm pellet was frozen in liquid nitrogen. Animals were
670 homogenized using Bullet Blender (Next Advance) in the presence of Qiazol Lysis Reagent
671 and 0.5mm Zirconia beads at 4°C. RNA was prepared using RNeasy Plus Universal Mini Kit
672 (Qiagen). Six independent RNA samples were prepared for each condition. The 2100
673 Bioanalyzer instrument (Agilent) was used for the RNA quality control with a microfluidic chip
674 specific for RNA (Agilent RNA 6000 Nano Kit). Then 1 μg of qualified RNA samples in
675 RNase-free ddH2O was used for library preparation. Library was constructed and sequenced
676 by Novogene.
677

678 **RNA-seq analysis**

679 The RNA-seq data were aligned using STAR v2.7.9a (Dobin et al., 2013) and gene expression
680 counts extracted by featureCounts v2.0.3 (Liao, Smyth, & Shi, 2014). Differential expression
681 was calculated using DESeq2 (Love, Huber, & Anders, 2014). GO analysis was performed
682 using the EnrichR R package (Kuleshov et al., 2016) on genes having p.adj < 1e-10. For brevity,
683 several highly similar GO categories were manually omitted (full EnrichR output available at
684 Github repository).

685

686 **Data availability**

687 Raw sequencing data has been deposited at ArrayExpress # E-MTAB-13296. The R code is
688 available at https://github.com/henriksson-lab/ce_h2s_tc.

689

690 **Acknowledgments**

691 We thank the Caenorhabditis Genetics Center (funded by NIH Office of Research Infrastructure
692 Programs P40 OD010440) and the National BioResources Project Japan for strains.

693

694 **Funding**

695 The computations were enabled by resources provided by the National Academic Infrastructure
696 for Supercomputing in Sweden (NAISS) and the Swedish National Infrastructure for
697 Computing (SNIC) at UPPMAX partially funded by the Swedish Research Council through
698 grant agreements no. 2022-06725 and no. 2018-05973. This work is supported by the Swedish
699 VR Research Council grant MIMS (2021-06602) to J.H., the Belgian National Fund for
700 Scientific Research (FRS-FNRS) to P.L., the ERC starting grant (802653 OXYGEN
701 SENSING), the Swedish Research Council VR starting grant (2018-02216), and the
702 Wallenberg Centre for Molecular Medicine (Umeå) to C.C.

703

704 **References**

Abel, D. C., Koenig, C. C., & Davis, W. P. (1987). Emersion in the Mangrove Forest Fish *Rivulus-Marmoratus* - a Unique Response to Hydrogen-Sulfide. *Environmental Biology of Fishes, 18*(1), 67-72. doi:Doi 10.1007/Bf00002329

Ackerman, D., & Gems, D. (2012). Insulin/IGF-1 and Hypoxia Signaling Act in Concert to Regulate Iron Homeostasis in *Caenorhabditis elegans*. *Plos Genetics, 8*(3). e1002498. doi: 10.1371/journal.pgen.1002498

Adams, D. F., Farwell, S. O., Pack, M. R., & Bamesberger, W. L. (1979). Preliminary Measurements of Biogenic Sulfur-Containing Gas Emissions from Soils. *Journal of the Air Pollution Control Association, 29*(4), 380-383. doi:10.1080/00022470.1979.10470805

Anderson, C. P., & Leibold, E. A. (2014). Mechanisms of iron metabolism in *Caenorhabditis elegans*. *Frontiers in Pharmacology, 5*. doi: 10.3389/fphar.2014.00113

Beets, I., Zhang, G., Fenk, L. A., Chen, C., Nelson, G. M., Felix, M. A., & de Bono, M. (2020). Natural Variation in a Dendritic Scaffold Protein Remodels Experience-Dependent Plasticity by Altering Neuropeptide Expression. *Neuron, 105*(1), 106-121 e110. doi:10.1016/j.neuron.2019.10.001

Brenner, S. (1974). The genetics of *Caenorhabditis elegans*. *Genetics, 77*(1), 71-94. Retrieved from https://www.ncbi.nlm.nih.gov/pubmed/4366476

Bretscher, A. J., Busch, K. E., & de Bono, M. (2008). A carbon dioxide avoidance behavior is integrated with responses to ambient oxygen and food in *Caenorhabditis elegans*. *Proc Natl Acad Sci U S A, 105*(23), 8044-8049. doi:10.1073/pnas.0707607105

Budde, M. W., & Roth, M. B. (2010). Hydrogen sulfide increases hypoxia-inducible factor-1 activity independently of von Hippel-Lindau tumor suppressor-1 in *C. elegans*. *Mol Biol Cell, 21*(1), 212-217. doi:10.1091/mbc.E09-03-0199

Budde, M. W., & Roth, M. B. (2011). The response of *Caenorhabditis elegans* to hydrogen sulfide and hydrogen cyanide. *Genetics, 189*(2), 521-532. doi:10.1534/genetics.111.129841

Busch, K. E., Laurent, P., Soltesz, Z., Murphy, R. J., Faivre, O., Hedwig, B., de Bono, M. (2012). Tonic signaling from O(2) sensors sets neural circuit activity and behavioral state. *Nat Neurosci, 15*(4), 581-591. doi:10.1038/nn.3061

Byrne Rodgers, J., & Ryu, W. S. (2020). Targeted thermal stimulation and high-content phenotyping reveal that the *C. elegans* escape response integrates current behavioral state and past experience. *PLoS One, 15*(3), e0229399. doi:10.1371/journal.pone.0229399

Carrillo, M. A., Guillermin, M. L., Rengarajan, S., Okubo, R. P., & Hallem, E. A. (2013). O-2-Sensing Neurons Control CO_2 Response in *C. elegans*. *Journal of Neuroscience, 33*(23), 9675-9683. doi:10.1523/Jneurosci.4541-12.2013

Chang, A. J., Chronis, N., Karow, D. S., Marletta, M. A., & Bargmann, C. I. (2006). A distributed chemosensory circuit for oxygen preference in *C. elegans*. *PLoS Biol, 4*(9), e274. doi:10.1371/journal.pbio.0040274

Cheung, B. H., Cohen, M., Rogers, C., Albayram, O., & de Bono, M. (2005). Experience-dependent modulation of *C. elegans* behavior by ambient oxygen. *Curr Biol, 15*(10), 905-917. doi:10.1016/j.cub.2005.04.017

Cooper, C. E., & Brown, G. C. (2008). The inhibition of mitochondrial cytochrome oxidase by the gases carbon monoxide, nitric oxide, hydrogen cyanide and hydrogen sulfide: chemical mechanism and physiological significance. *J Bioenerg Biomembr, 40*(5), 533-539. doi:10.1007/s10863-008-9166-6

Couto, A., Oda, S., Nikolaev, V. O., Soltesz, Z., & de Bono, M. (2013). In vivo genetic dissection of O_2-evoked cGMP dynamics in a *Caenorhabditis elegans* gas sensor. *Proc Natl Acad Sci U S A, 110*(35), E3301-3310. doi:10.1073/pnas.1217428110

de Bono, M., & Bargmann, C. I. (1998). Natural variation in a neuropeptide Y receptor homolog modifies social behavior and food response in *C. elegans*. *Cell, 94*(5), 679-689. doi:10.1016/s0092-8674(00)81609-8

758 Dekker, L. V., Mcintyre, P., & Parker, P. J. (1993). Mutagenesis of the Regulatory Domain of
759 Rat Protein Kinase-C-Eta - a Molecular-Basis for Restricted Histone Kinase-Activity.
760 *Journal of Biological Chemistry, 268*(26), 19498-19504.
761 Dev, S., & Babitt, J. L. (2017). Overview of iron metabolism in health and disease. *Hemodial*
762 *Int, 21 Suppl 1*(Suppl 1), S6-S20. doi:10.1111/hdi.12542
763 Dobin, A., Davis, C. A., Schlesinger, F., Drenkow, J., Zaleski, C., Jha, S., Gingeras, T. R.
764 (2013). STAR: ultrafast universal RNA-seq aligner. *Bioinformatics, 29*(1), 15-21.
765 doi:10.1093/bioinformatics/bts635
766 Dokshin, G. A., Ghanta, K. S., Piscopo, K. M., & Mello, C. C. (2018). Robust Genome
767 Editing with Short Single-Stranded and Long, Partially Single-Stranded DNA Donors
768 in *Caenorhabditis elegans*. *Genetics, 210*(3), 781-787.
769 doi:10.1534/genetics.118.301532
770 Doonan, R., McElwee, J. J., Matthijssens, F., Walker, G. A., Houthoofd, K., Back, P., Gems,
771 D. (2008). Against the oxidative damage theory of aging: superoxide dismutases
772 protect against oxidative stress but have little or no effect on life span in
773 *Caenorhabditis elegans*. *Genes Dev, 22*(23), 3236-3241. doi:10.1101/gad.504808
774 Fawcett, E. M., Hoyt, J. M., Johnson, J. K., & Miller, D. L. (2015). Hypoxia disrupts
775 proteostasis in *Caenorhabditis elegans*. *Aging Cell, 14*(1), 92-101.
776 doi:10.1111/acel.12301
777 Ferkey, D. M., Sengupta, P., & L'Etoile, N. D. (2021). Chemosensory signal transduction in
778 *Caenorhabditis elegans*. *Genetics, 217*(3). doi:10.1093/genetics/iyab004
779 Gao, L., Gonzalez-Rodriguez, P., Ortega-Saenz, P., & Lopez-Barneo, J. (2017). Redox
780 signaling in acute oxygen sensing. *Redox Biol, 12*, 908-915.
781 doi:10.1016/j.redox.2017.04.033
782 Gea, T., Barrena, R., Artola, A., & Sanchez, A. (2004). Monitoring the biological activity of
783 the composting process: Oxygen uptake rate (OUR), respirometric index (RI), and
784 respiratory quotient (RQ). *Biotechnol Bioeng, 88*(4), 520-527. doi:10.1002/bit.20281

785 Ghanta, K. S., & Mello, C. C. (2020). Melting dsDNA Donor Molecules Greatly Improves
786 Precision Genome Editing in *Caenorhabditis elegans*. *Genetics, 216*(3), 643-650.
787 doi:10.1534/genetics.120.303564
788 Gourley, B. L., Parker, S. B., Jones, B. J., Zumbrennen, K. B., & Leibold, E. A. (2003).
789 Cytosolic aconitase and ferritin are regulated by iron in *Caenorhabditis elegans*. *J*
790 *Biol Chem, 278*(5), 3227-3234. doi:10.1074/jbc.M210333200
791 Gray, J. M., Karow, D. S., Lu, H., Chang, A. J., Chang, J. S., Ellis, R. E., Bargmann, C. I.
792 (2004). Oxygen sensation and social feeding mediated by a *C. elegans* guanylate
793 cyclase homologue. *Nature, 430*(6997), 317-322. doi:10.1038/nature02714
794 Hallem, E. A., Spencer, W. C., McWhirter, R. D., Zeller, G., Henz, S. R., Ratsch, G.,
795 Ringstad, N. (2011). Receptor-type guanylate cyclase is required for carbon dioxide
796 sensation by *Caenorhabditis elegans*. *Proc Natl Acad Sci U S A, 108*(1), 254-259.
797 doi:10.1073/pnas.1017354108
798 Hallem, E. A., & Sternberg, P. W. (2008). Acute carbon dioxide avoidance in *Caenorhabditis*
799 *elegans*. *Proc Natl Acad Sci U S A, 105*(23), 8038-8043.
800 doi:10.1073/pnas.0707469105
801 Heiman, M. G., & Shaham, S. (2009). DEX-1 and DYF-7 establish sensory dendrite length
802 by anchoring dendritic tips during cell migration. *Cell, 137*(2), 344-355.
803 doi:10.1016/j.cell.2009.01.057
804 Hentze, M. W., Muckenthaler, M. U., & Andrews, N. C. (2004). Balancing acts: molecular
805 control of mammalian iron metabolism. *Cell, 117*(3), 285-297. doi:10.1016/s0092-
806 8674(04)00343-5
807 Hildebrandt, T. M., & Grieshaber, M. K. (2008). Three enzymatic activities catalyze the
808 oxidation of sulfide to thiosulfate in mammalian and invertebrate mitochondria.
809 *FEBS J, 275*(13), 3352-3361. doi:10.1111/j.1742-4658.2008.06482.x
810 Hiroki, S., Yoshitane, H., Mitsui, H., Sato, H., Umatani, C., Kanda, S., Iino, Y. (2022).
811 Molecular encoding and synaptic decoding of context during salt chemotaxis in *C.*
812 *elegans*. *Nature Communications, 13*(1). doi:10.1038/s41467-022-30279-7

Horsman, J. W., Heinis, F. I., & Miller, D. L. (2019). A Novel Mechanism To Prevent H_2S Toxicity in *Caenorhabditis elegans*. *Genetics, 213*(2), 481-490. doi:10.1534/genetics.119.302326

Horsman, J. W., & Miller, D. L. (2016). Mitochondrial Sulfide Quinone Oxidoreductase Prevents Activation of the Unfolded Protein Response in Hydrogen Sulfide. *J Biol Chem, 291*(10), 5320-5325. doi:10.1074/jbc.M115.697102

Jackson, M. R., Melideo, S. L., & Jorns, M. S. (2012). Human sulfide:quinone oxidoreductase catalyzes the first step in hydrogen sulfide metabolism and produces a sulfane sulfur metabolite. *Biochemistry, 51*(34), 6804-6815. doi:10.1021/bi300778t

Jia, J., Wang, Z., Zhang, M., Huang, C., Song, Y., Xu, F., Cheng, J. (2020). SQR mediates therapeutic effects of H(2)S by targeting mitochondrial electron transport to induce mitochondrial uncoupling. *Sci Adv, 6*(35), eaaz5752. doi:10.1126/sciadv.aaz5752

Kabil, O., & Banerjee, R. (2012). Characterization of patient mutations in human persulfide dioxygenase (ETHE1) involved in H_2S catabolism. *J Biol Chem, 287*(53), 44561-44567. doi:10.1074/jbc.M112.407411

Kaelin, W. G., Jr., & Ratcliffe, P. J. (2008). Oxygen sensing by metazoans: the central role of the HIF hydroxylase pathway. *Mol Cell, 30*(4), 393-402. doi:10.1016/j.molcel.2008.04.009

Kelley, J. L., Arias-Rodriguez, L., Patacsil Martin, D., Yee, M. C., Bustamante, C. D., & Tobler, M. (2016). Mechanisms Underlying Adaptation to Life in Hydrogen Sulfide-Rich Environments. *Mol Biol Evol, 33*(6), 1419-1434. doi:10.1093/molbev/msw020

Khan, A. A., Schuler, M. M., Prior, M. G., Yong, S., Coppock, R. W., Florence, L. Z., & Lillie, L. E. (1990). Effects of hydrogen sulfide exposure on lung mitochondrial respiratory chain enzymes in rats. *Toxicol Appl Pharmacol, 103*(3), 482-490. doi:10.1016/0041-008x(90)90321-k

Kodama-Namba, E., Fenk, L. A., Bretscher, A. J., Gross, E., Busch, K. E., & de Bono, M. (2013). Cross-modulation of homeostatic responses to temperature, oxygen and

840 carbon dioxide in *C. elegans*. *PLoS Genet, 9*(12), e1004011.
841 doi:10.1371/journal.pgen.1004011
842 Kuleshov, M. V., Jones, M. R., Rouillard, A. D., Fernandez, N. F., Duan, Q. N., Wang, Z. C.,
843 Ma'ayan, A. (2016). Enrichr: a comprehensive gene set enrichment analysis web
844 server 2016 update. *Nucleic Acids Research, 44*(W1), W90-W97.
845 doi:10.1093/nar/gkw377
846 Laurent, P., Soltesz, Z., Nelson, G. M., Chen, C., Arellano-Carbajal, F., Levy, E., & de Bono,
847 M. (2015). Decoding a neural circuit controlling global animal state in *C. elegans*.
848 *Elife, 4*. doi:10.7554/eLife.04241
849 Lee, S. J., Hwang, A. B., & Kenyon, C. (2010). Inhibition of Respiration Extends *C. elegans*
850 Life Span via Reactive Oxygen Species that Increase HIF-1 Activity. *Current*
851 *Biology, 20*(23), 2131-2136. doi:10.1016/j.cub.2010.10.057
852 Lennicke, C., & Cocheme, H. M. (2021). Redox metabolism: ROS as specific molecular
853 regulators of cell signaling and function. *Mol Cell, 81*(18), 3691-3707.
854 doi:10.1016/j.molcel.2021.08.018
855 Liao, Y., Smyth, G. K., & Shi, W. (2014). featureCounts: an efficient general purpose
856 program for assigning sequence reads to genomic features. *Bioinformatics, 30*(7),
857 923-930. doi:10.1093/bioinformatics/btt656
858 Liochev, S. L. (1996). The role of iron-sulfur clusters in in vivo hydroxyl radical production.
859 *Free Radical Research, 25*(5), 369-384. doi:Doi 10.3109/10715769609149059
860 Love, M. I., Huber, W., & Anders, S. (2014). Moderated estimation of fold change and
861 dispersion for RNA-seq data with DESeq2. *Genome Biology, 15*(12). doi:
862 10.1186/s13059-014-0550-8
863 Ma, D. K., Vozdek, R., Bhatla, N., & Horvitz, H. R. (2012). CYSL-1 interacts with the O_2-
864 sensing hydroxylase EGL-9 to promote H_2S-modulated hypoxia-induced behavioral
865 plasticity in *C. elegans*. *Neuron, 73*(5), 925-940. doi:10.1016/j.neuron.2011.12.037
866 Macosko, E. Z., Pokala, N., Feinberg, E. H., Chalasani, S. H., Butcher, R. A., Clardy, J., &
867 Bargmann, C. I. (2009). A hub-and-spoke circuit drives pheromone attraction and

social behaviour in *C. elegans*. *Nature, 458*(7242), 1171-1175. doi:10.1038/nature07886

Mathew, N. D., Schlipalius, D. I., & Ebert, P. R. (2011). Sulfurous gases as biological messengers and toxins: comparative genetics of their metabolism in model organisms. *J Toxicol, 2011*, 394970. doi:10.1155/2011/394970

McGrath, P. T., Rockman, M. V., Zimmer, M., Jang, H., Macosko, E. Z., Kruglyak, L., & Bargmann, C. I. (2009). Quantitative mapping of a digenic behavioral trait implicates globin variation in *C. elegans* sensory behaviors. *Neuron, 61*(5), 692-699. doi:10.1016/j.neuron.2009.02.012

Miller, D. L., Budde, M. W., & Roth, M. B. (2011). HIF-1 and SKN-1 Coordinate the Transcriptional Response to Hydrogen Sulfide in *Caenorhabditis elegans*. *PLoS One, 6*(9). doi: 10.1371/journal.pone.0025476

Miller, D. L., & Roth, M. B. (2007). Hydrogen sulfide increases thermotolerance and lifespan in *Caenorhabditis elegans*. *Proc Natl Acad Sci U S A, 104*(51), 20618-20622. doi:10.1073/pnas.0710191104

Morra, M. J., & Dick, W. A. (1991). Mechanisms of h(2)s production from cysteine and cystine by microorganisms isolated from soil by selective enrichment. *Appl Environ Microbiol, 57*(5), 1413-1417. doi:10.1128/aem.57.5.1413-1417.1991

Murakami, M., Koga, M., & Ohshima, Y. (2001). DAF-7/TGF-beta expression required for the normal larval development in *C. elegans* is controlled by a presumed guanylyl cyclase DAF-11. *Mechanisms of Development, 109*(1), 27-35. doi: 10.1016/S0925-4773(01)00507-X

Murayama, T., Toh, Y., Ohshima, Y., & Koga, M. (2005). The *dyf-3* gene encodes a novel protein required for sensory cilium formation in *Caenorhabditis elegans*. *J Mol Biol, 346*(3), 677-687. doi:10.1016/j.jmb.2004.12.005

Myllyharju, J., & Kivirikko, K. I. (1997). Characterization of the iron- and 2-oxoglutarate-binding sites of human prolyl 4-hydroxylase. *Embo Journal, 16*(6), 1173-1180. doi: 10.1093/emboj/16.6.1173

896 Nicholls, P., & Kim, J. K. (1982). Sulphide as an inhibitor and electron donor for the
897 cytochrome *c* oxidase system. *Can J Biochem, 60*(6), 613-623. doi:10.1139/o82-076
898 Niu, W., Lu, Z. J., Zhong, M., Sarov, M., Murray, J. I., Brdlik, C. M., Reinke, V. (2011).
899 Diverse transcription factor binding features revealed by genome-wide ChIP-seq in
900 *C. elegans*. *Genome Research, 21*(2), 245-254. doi:10.1101/gr.114587.110
901 Ochi, R., Dhagia, V., Lakhkar, A., Patel, D., Wolin, M. S., & Gupte, S. A. (2016). Rotenone-
902 stimulated superoxide release from mitochondrial complex I acutely augments L-type
903 Ca^{2+} current in A7r5 aortic smooth muscle cells. *Am J Physiol Heart Circ Physiol,*
904 *310*(9), H1118-1128. doi:10.1152/ajpheart.00889.2015
905 Olson, K. R., & Straub, K. D. (2016). The Role of Hydrogen Sulfide in Evolution and the
906 Evolution of Hydrogen Sulfide in Metabolism and Signaling. *Physiology (Bethesda),*
907 *31*(1), 60-72. doi:10.1152/physiol.00024.2015
908 Onukwufor, J. O., Farooqi, M. A., Vodickova, A., Koren, S. A., Baldzizhar, A., Berry, B. J.,
909 Wojtovich, A. P. (2022). A reversible mitochondrial complex I thiol switch mediates
910 hypoxic avoidance behavior in *C. elegans*. *Nat Commun, 13*(1), 2403.
911 doi:10.1038/s41467-022-30169-y
912 Oshins, C., Michel, F., Louis, P., Richard, T. L., & Rynk, R. (2022). Chapter 3 - The
913 composting process. In R. Rynk (Ed.), *The Composting Handbook* (pp. 51-101):
914 Academic Press.
915 Patange, O., Breen, P., Arsuffi, G., & Ruvkun, G. (2025). Hydrogen sulfide mediates the
916 interaction between *C. elegans* and Actinobacteria from its natural microbial
917 environment. *Cell Reports, 44*(1), 115170. doi:10.1016/j.celrep.2024.115170
918 Patten, D. A., Germain, M., Kelly, M. A., & Slack, R. S. (2010). Reactive oxygen species:
919 stuck in the middle of neurodegeneration. *J Alzheimers Dis, 20 Suppl 2*, S357-367.
920 doi:10.3233/JAD-2010-100498
921 Persson, A., Gross, E., Laurent, P., Busch, K. E., Bretes, H., & de Bono, M. (2009). Natural
922 variation in a neural globin tunes oxygen sensing in wild *Caenorhabditis elegans*.
923 *Nature, 458*(7241), 1030-1033. doi:10.1038/nature07820

924 Pettinati, I., Brem, J., McDonough, M. A., & Schofield, C. J. (2015). Crystal structure of
925 human persulfide dioxygenase: structural basis of ethylmalonic encephalopathy. *Hum*
926 *Mol Genet, 24*(9), 2458-2469. doi:10.1093/hmg/ddv007
927 Pfenninger, M., Lerp, H., Tobler, M., Passow, C., Kelley, J. L., Funke, E., Plath, M. (2014).
928 Parallel evolution of cox genes in H_2S-tolerant fish as key adaptation to a toxic
929 environment. *Nat Commun, 5*, 3873. doi:10.1038/ncomms4873
930 Philipp, T. M., Gong, W., Kohnlein, K., Ohse, V. A., Muller, F. I., Priebs, J., Klotz, L. O.
931 (2022). SEMO-1, a novel methanethiol oxidase in *Caenorhabditis elegans*, is a pro-
932 aging factor conferring selective stress resistance. *Biofactors, 48*(3), 699-706.
933 doi:10.1002/biof.1836
934 Powell-Coffman, J. A. (2010). Hypoxia signaling and resistance in *C. elegans*. *Trends*
935 *Endocrinol Metab, 21*(7), 435-440. doi:10.1016/j.tem.2010.02.006
936 Qabazard, B., Li, L., Gruber, J., Peh, M. T., Ng, L. F., Kumar, S. D., Moore, P. K. (2014).
937 Hydrogen sulfide is an endogenous regulator of aging in *Caenorhabditis elegans*.
938 *Antioxid Redox Signal, 20*(16), 2621-2630. doi:10.1089/ars.2013.5448
939 Rajan, M., Anderson, C. P., Rindler, P. M., Romney, S. J., Ferreira Dos Santos, M. C., Gertz,
940 J., & Leibold, E. A. (2019). NHR-14 loss of function couples intestinal iron uptake
941 with innate immunity in *C. elegans* through PQM-1 signaling. *Elife, 8*.
942 doi:10.7554/eLife.44674
943 Ramsay, R. R., & Singer, T. P. (1992). Relation of superoxide generation and lipid
944 peroxidation to the inhibition of NADH-Q oxidoreductase by rotenone, piericidin A,
945 and MPP+. *Biochem Biophys Res Commun, 189*(1), 47-52. doi:10.1016/0006-
946 291x(92)91523-s
947 Read, A. D., Bentley, R. E. T., Archer, S. L., & Dunham-Snary, K. J. (2021). Mitochondrial
948 iron-sulfur clusters: Structure, function, and an emerging role in vascular biology.
949 *Redox Biology, 47*. doi: 10.1016/j.redox.2021.102164

Rodriguez-Kabana, R., Jordan, J. W., & Hollis, J. P. (1965). Nematodes: Biological Control in Rice Fields: Role of Hydrogen Sulfide. *Science, 148*(3669), 524-526. doi:10.1126/science.148.3669.524

Romanelli-Cedrez, L., Vairoletti, F., & Salinas, G. (2024). Rhodoquinone-dependent electron transport chain is essential for *Caenorhabditis elegans* survival in hydrogen sulfide environments. *J Biol Chem, 300*(9), 107708. doi:10.1016/j.jbc.2024.107708

Romney, S. J., Newman, B. S., Thacker, C., & Leibold, E. A. (2011). HIF-1 regulates iron homeostasis in *Caenorhabditis elegans* by activation and inhibition of genes involved in iron uptake and storage. *PLoS Genet, 7*(12), e1002394. doi:10.1371/journal.pgen.1002394

Salvanes, A. G. V., Utne-Palm, A. C., Currie, B., & Braithwaite, V. A. (2011). Behavioural and physiological adaptations of the bearded goby, a key fish species of the extreme environment of the northern Benguela upwelling. *Marine Ecology Progress Series, 425*, 193-202. doi:10.3354/meps08998

Schiavo, G., Benfenati, F., Poulain, B., Rossetto, O., Polverino de Laureto, P., DasGupta, B. R., & Montecucco, C. (1992). Tetanus and botulinum-B neurotoxins block neurotransmitter release by proteolytic cleavage of synaptobrevin. *Nature, 359*(6398), 832-835. doi:10.1038/359832a0

Semenza, G. L. (2010). Defining the role of hypoxia-inducible factor 1 in cancer biology and therapeutics. *Oncogene, 29*(5), 625-634. doi:10.1038/onc.2009.441

Starich, T. A., Herman, R. K., Kari, C. K., Yeh, W. H., Schackwitz, W. S., Schuyler, M. W., Riddle, D. L. (1995). Mutations affecting the chemosensory neurons of *Caenorhabditis elegans*. *Genetics, 139*(1), 171-188. doi:10.1093/genetics/139.1.171

Sterken, M. G., Snoek, L. B., Kammenga, J. E., & Andersen, E. C. (2015). The laboratory domestication of *Caenorhabditis elegans*. *Trends Genet, 31*(5), 224-231. doi:10.1016/j.tig.2015.02.009

976 Swoboda, P., Adler, H. T., & Thomas, J. H. (2000). The RFX-type transcription factor DAF-
977 19 regulates sensory neuron cilium formation in *C. elegans*. *Mol Cell, 5*(3), 411-421.
978 doi:10.1016/s1097-2765(00)80436-0
979 Szabo, C., Ransy, C., Módis, K., Andriamihaja, M., Murghes, B., Coletta, C., Bouillaud, F.
980 (2014). Regulation of mitochondrial bioenergetic function by hydrogen sulfide. Part
981 I. Biochemical and physiological mechanisms. *British Journal of Pharmacology,*
982 *171*(8), 2099-2122. doi:10.1111/bph.12369
983 Topalidou, I., & Miller, D. L. (2017). *Caenorhabditis elegans* HIF-1 Is Broadly Required for
984 Survival in Hydrogen Sulfide. *G3 (Bethesda), 7*(11), 3699-3704.
985 doi:10.1534/g3.117.300146
986 Vora, M., Pyonteck, S. M., Popovitchenko, T., Matlack, T. L., Prashar, A., Kane, N. S.,
987 Rongo, C. (2022). The hypoxia response pathway promotes PEP carboxykinase and
988 gluconeogenesis in *C. elegans*. *Nature Communications, 13*(1). doi: 10.1038/s41467-
989 022-33849-x
990 Weir, E. K., Lopez-Barneo, J., Buckler, K. J., & Archer, S. L. (2005). Acute oxygen-sensing
991 mechanisms. *N Engl J Med, 353*(19), 2042-2055. doi:10.1056/NEJMra050002
992 Xu, X. M., & Moller, S. G. (2011). Iron-Sulfur Clusters: Biogenesis, Molecular Mechanisms,
993 and Their Functional Significance. *Antioxidants & Redox Signaling, 15*(1), 271-307.
994 doi:10.1089/ars.2010.3259
995 Zhao, L., Fenk, L. A., Nilsson, L., Amin-Wetzel, N. P., Ramirez-Suarez, N. J., de Bono, M.,
996 & Chen, C. (2022). ROS and cGMP signaling modulate persistent escape from
997 hypoxia in *Caenorhabditis elegans*. *PLoS Biol, 20*(6), e3001684.
998 doi:10.1371/journal.pbio.3001684
999 Zimmer, M., Gray, J. M., Pokala, N., Chang, A. J., Karow, D. S., Marletta, M. A., Bargmann,
1000 C. I. (2009). Neurons detect increases and decreases in oxygen levels using distinct
1001 guanylate cyclases. *Neuron, 61*(6), 865-879. doi:10.1016/j.neuron.2009.02.013

1002 Zorov, D. B., Juhaszova, M., & Sollott, S. J. (2014). Mitochondrial reactive oxygen species
1003 (ROS) and ROS-induced ROS release. *Physiol Rev, 94*(3), 909-950.
1004 doi:10.1152/physrev.00026.2013
1005 Zubovych, I. O., Straud, S., & Roth, M. G. (2010). Mitochondrial dysfunction confers
1006 resistance to multiple drugs in *Caenorhabditis elegans*. *Mol Biol Cell, 21*(6), 956-
1007 969. doi:10.1091/mbc.e09-08-0673
1008

1009 **Figure legends**

1010 **Figure 1. Acute locomotory responses of *C. elegans* to hydrogen sulfide**

1011 (**A**) Changes in the locomotory speed of WT animals (N2 laboratory strain) evoked by a switch
1012 from 7% O_2 to 150 ppm H_2S balanced with 7% O_2, followed by a return to 7% O_2. (**B**)
1013 Proportion of WT animals undergoing reorientation movements (omega turns) during a switch
1014 from 7% O_2 to 150 ppm H_2S balanced with 7% O_2, followed by a return to 7% O_2. (**C**) Fraction
1015 of WT animals doing backward locomotion (reversals) during a switch from 7% O_2 to 150 ppm
1016 H_2S balanced with 7% O_2, followed by a return to 7% O_2. (**D**) Locomotory speed of WT was
1017 recorded for 2 minutes at 7% O_2, followed by 148 minutes at 150 ppm H_2S balanced with 7%
1018 O_2, and then at 7% O_2. (**E**) Locomotory speed of WT animals in response to near-UV light (435
1019 nm, 0.7 mW/mm^2) exposure, before and directly after 30-minute preincubation in 150 ppm H_2S
1020 balanced with 7% O_2. Locomotory activity was recorded for 2 minutes before, during and after
1021 UV light exposure. (**F**) Locomotory speed of WT animals to different concentrations of H_2S
1022 balanced with 7% O_2. Red bars on the x-axis represent two intervals (4–5 minutes and 11–12
1023 minutes, labeled a and b, respectively) used for statistical analysis. **** = $p < 0.0001$, ** = $p <$
1024 0.01, * = $p < 0.05$, ns = not significant, Mann–Whitney U test. (**G**) Distribution of WT animals
1025 in a microfluidic device after 25 minutes of aerotaxis. The gas inputs and the five chamber
1026 sections used for scoring are indicated. (**H**) Distribution of WT animals in a gradient of H_2S
1027 (150 ppm to 0 ppm). The bins correspond to different sections of the microfluidic chamber
1028 described in (**G**). N= 4 aerotaxis assays.
1029

1030 **Figure 2. Neurosecretion from ASJ neurons contributes to H_2S avoidance**

1031 (**A–H**) Locomotory speed responses to a switch from 7% O_2 to 150 ppm H_2S balanced with 7%
1032 O_2 for animals of the indicated genotype: WT and *daf-19(m86)* (**A**); WT and *dyf-3(m185)* (**B**);
1033 WT and *dyf-7(m539)* (**C**); WT, *daf-11(m47)* and *tax-4(p678)* (**D**); WT and *tax-2(p691)* (**E**);
1034 WT, *daf-11(m47)* and transgenic *daf-11(m47)* expressing *daf-11* genomic DNA in ASJ neurons
1035 (two independent lines) (**F**); WT, *tax-4(p678)* and transgenic *tax-4(p678)* expressing *tax-4*
1036 cDNA in ASJ neurons (two independent lines) (**G**); WT and transgenic WT expressing the
1037 catalytic domain of the *tetanus* toxin (TeTx) in ASJ neurons (**H**). For the comparison of acute
1038 locomotory speed responses between strains, red bars on the x-axis represent two intervals (4–
1039 5 minutes and 11–12 minutes, labeled a and b, respectively, in panels D, F, and G) used for
1040 statistical analysis. **** = $p < 0.0001$, *** = $p < 0.001$, ** = $p < 0.01$, * = $p < 0.05$, ns = not
1041 significant, Mann–Whitney U test. (**I**) Calcium transients evoked in ASJ neurons of WT
1042 animals in response to a switch from 7% O_2 to 150 ppm H_2S balanced with 7% O_2 for animals
1043 (N=42). The slow decline in GCaMP6s fluorescence is due to photobleaching.

1044

1045 **Figure 3. Insulin, TGF-β, and high O_2 signaling pathways antagonizes H_2S avoidance**

1046 (**A, B**) Locomotory speed responses to a switch from 7% O_2 to 150 ppm H_2S balanced with 7%
1047 O_2 for animals of the indicated genotype: WT, *daf-2(e1370), daf-16(mgDf47)*, and *daf-2(e1370);*
1048 *daf-16(mgDf47)* double mutants (**A**); WT, *daf-7(e1372), daf-3(mgDf90),* and *daf-7(e1372);*
1049 *daf-3(mgDf90)* double mutants (**B**). For the *daf-2* assays, WT and *daf-2* mutants were
1050 maintained at 15°C. L4 animals were picked and shifted to 25°C until day-one adults, then
1051 assayed at room temperature. (**C**) Hypothetical model for the regulation of H_2S avoidance by a
1052 starvation program involving the insulin, TGF-β, and NHR-49 pathways. (**D**) Locomotory
1053 speed response to a switch from 7% O_2 to 150 ppm H_2S balanced with 7% O_2 in fed and starved
1054 WT animals. (**E, F**) Locomotory speed responses to a switch from 7% O_2 to 150 ppm H_2S
1055 balanced with 7% O_2 for animals of the indicated genotype: WT and wild isolates (CB4858 and
1056 CB4855) (**E**); WT and *npr-1(ad609)* (**F**). (**G**) Hypothetical model showing how O_2 regulates
1057 H_2S avoidance via the inhibitory RMG circuit activity, which is modulated by O_2 sensory inputs

1058 and NPR-1 signaling. (**H–L**) Locomotory speed responses to a switch from 7% O_2 to 150 ppm
1059 H_2S balanced with 7% O_2 for animals of the indicated genotype: WT, *npr-1(ad609)*, and
1060 transgenic *npr-1(ad609)* expressing *npr-1* in RMG neurons using Cre-LoxP system (Macosko
1061 et al., 2009) (**H**); WT, *npr-1(ad609), gcy-35(ok769)*, and *npr-1(ad609); gcy-35(ok769)* double
1062 mutants (**I**); WT, *npr-1(ad609), tax-4(p678)* and *npr-1(ad609); tax-4(p678)* double mutants (**J**);
1063 WT, *npr-1(ad609), qaIs2241*(genetic ablation of AQR, PQR and URX neurons) and *npr-*
1064 *1(ad609); qaIs 2241* (**K**); WT, *npr-1(ad609), npr-1(ad609); gcy-35(ok769)* double mutants and
1065 *transgenic npr-1(ad609); gcy-35(ok769)* double mutants expressing *gcy-35* cDNA under *gcy-*
1066 *37* promoter, which drives *gcy-35* expression in O_2 sensing neurons (**L**). For the comparison of
1067 acute locomotory responses between strains, red bars on the x-axis represent two intervals (4–
1068 5 minutes and 11–12 minutes, labeled a and b, respectively, in panel E) used for statistical
1069 analysis. **** = $p < 0.0001$, *** = $p < 0.001$, ** = $p < 0.01$, * = $p < 0.05$, ns = not significant,
1070 Mann–Whitney U test.
1071
1072 **Figure 4. Prolonged H_2S exposure reprograms gene expression in *C. elegans***
1073 (**A**) Venn diagram displaying the number of differentially expressed genes after 1-hour
1074 exposure to 50 ppm or 150 ppm H_2S balanced with 7% O_2 in WT animals (adjusted $p < 1e-10$).
1075 (**B**) Venn diagram displaying the number of differentially expressed genes after 1-, 2-, and 12-
1076 hour exposure to 150 ppm H_2S balanced with 7% O_2 in WT animals (adjusted $p < 1e-10$). (**C,**
1077 **D**) Significantly enriched GO categories for differentially expressed genes with adjusted $p <$
1078 1e-10 in WT animals exposed to 50 ppm (**C**) or 150 ppm (**D**) H_2S balanced with 7% O_2 for 1
1079 hour. (**E, F**) Volcano plots showing the differentially expressed genes with adjusted $p < 1e-10$
1080 in WT animals exposed to 50 ppm (**E**) or 150 ppm (**F**) H_2S balanced with 7% O_2 for 1 hour. A
1081 set of genes involved in H_2S detoxification, cysteine metabolism and stress response were
1082 highlighted in red.
1083
1084 **Figure 5. Acute response to H_2S is modulated by HIF-1 signaling**

1085 (**A**) Locomotory speed responses of WT animals to a switch from 7% O_2 to 150 ppm H_2S
1086 balanced with 7% O_2 after incubation of the animals for 0, 12, 24, or 36 hours in 1% O_2. (**B, C**)
1087 Locomotory speed responses to a switch from 7% O_2 to 150 ppm H_2S balanced with 7% O_2 for
1088 animals of the indicated genotype: WT, *egl-9(sa307)*, and *vhl-1(ok161)* (**B**); WT and transgenic
1089 animals expressing the non-degradable form of HIF-1 (P621A or P621G) under the pan-
1090 neuronal *unc-14* promoter or the endogenous *hif-1* promoter, respectively (**C**). (**D–F**)
1091 Avoidance responses of WT and *hif-1(ia4)* to a switch from 7% O_2 to 150 ppm H_2S balanced
1092 with 7% O_2, including locomotory speed (**D**), reorientation (omega-turn) (**E**), and reversal (**F**).
1093 (**G, H**) Locomotory speed responses to a switch from 7% O_2 to 150 ppm H_2S balanced with 7%
1094 O_2 for animals of the indicated genotype: WT, *egl-9(sa307), hif-1(ia4)*, and *egl-9(sa307); hif-*
1095 *1(ia4)* double mutants (**G**); WT, *vhl-1(ok161), hif-1(ia4)*, and *vhl-1(ok161); hif-1(ia4)* double
1096 mutants (**H**). (**I**) Average locomotory speed during 2 minutes of exposure to near-UV light for
1097 WT, *hif-1(ia4)*, and *egl-9(sa307)* before (Ctrl = control) and after 30 minutes of exposure to
1098 150 ppm H_2S balanced with 7% O_2. (**J–L**) Locomotory speed responses to a switch from 7%
1099 O_2 to 150 ppm H_2S balanced with 7% O_2 for animals of the indicated genotype: WT and *sqrd-*
1100 *1(tm3378)* (**J**); WT and *ethe-1(yum2895)* (**K**); WT, *cysl-1(ok762), cysl-2(ok3516)*, and *cysl-*
1101 *3(yum4)* (**L**). For the comparison of acute locomotory responses between strains, red bars on
1102 the x-axis represent two intervals (4–5 minutes and 11–12 minutes, labeled a and b, respectively,
1103 in panels A, B, C, and L) used for statistical analysis. *** = $p < 0.001$, ** = $p < 0.01$, * = $p <$
1104 0.05, ns = not significant, Mann–Whitney U test.
1105

1106 **Figure 6. Labile iron pool sustains the locomotory activity in H_2S**

1107 (**A, B**) Volcano plots showing the relative expression of the genes involved in the regulation of
1108 iron homeostasis in WT animals after 2-hour exposure in 50 ppm (**A**) or 150 ppm (**B**) H_2S
1109 balanced with 7% O_2. (**C–G**) Locomotory speed responses to a switch from 7% O_2 to 150 ppm
1110 H_2S balanced with 7% O_2 for animals of indicated genotypes or treatments: WT and animals
1111 overexpressing *ftn-1* genomic DNA under its own promoter (#1 and #2 indicate two
1112 independent lines) (**C**); WT, *smf-3(ok1305)*, and *ftn-1(ok3625)* (**D**); WT, and WT pretreated

1113 with 100 μM 2,2′-Bipyridyl (BP) or with 5 mg/ml ferric ammonium citrate (FAC) in the
1114 presence of food for 16 hours (**E**); WT, *hif-1(ia4)*, and *hif-1(ia4)* mutants pretreated with 5
1115 mg/ml ferric ammonium citrate (FAC) for 16 hours (**F**); WT, *hif-1(ia4), ftn-1(ok3625)*, and *hif-*
1116 *1(ia4); ftn-1(ok3625)* double mutants (**G**). (**H**) Hypothetical model of the interactions between
1117 labile iron pool and HIF-1 signaling. For the comparison of acute locomotory speed responses
1118 between strains or conditions, red bars on the x-axis represent two intervals (4–5 minutes and
1119 11–12 minutes, labeled a and b, respectively, in panels C, D, and E) used for statistical analysis.
1120 **** = $p < 0.0001$, *** = $p < 0.001$, ** = $p < 0.01$, * = $p < 0.05$, ns = not significant, Mann–
1121 Whitney U test.
1122
1123 **Figure 7. Mitochondrial function is required for acute response to H_2S**
1124 (**A–D**) Locomotory speed responses to a switch from 7% O_2 to 150 ppm H_2S balanced with 7%
1125 O_2 for animals of the indicated genotype: WT and *gas-1(fc21)* (**A**); WT and *clk-1(qm30)* (**B**);
1126 WT and *mev-1(kn1)* (**C**); WT and *isp-1(qm150)* (**D**). (**E**) Locomotory speed responses to a
1127 switch from 7% O_2 to 150 ppm H_2S balanced with 7% O_2 for WT animals pretreated with 10
1128 μM rotenone for 0 minute, 10 minutes, 30 minutes, 60 minutes or 120 minutes. For the
1129 comparison of acute locomotory speed responses between strains or conditions, red bars on the
1130 x-axis represent two intervals (4–5 minutes and 11–12 minutes) used for statistical analysis.
1131 *** = $p < 0.001$, ** = $p < 0.01$, * = $p < 0.05$, ns = not significant, Mann–Whitney U test. (**F–**
1132 **G**) Locomotory speed responses to a switch from 7% O_2 to 150 ppm H_2S balanced with 7% O_2
1133 for animals of the indicated genotype: WT, *sod-1(tm776)*, *sod-2(ok1030)*, and *sod-3(tm760)*
1134 (**F**); WT, *sod-4(gk101)*, *sod-5(tm1146)*, and *sod-1(tm783); sod-2(ok1030); sod-3(tm760); sod-*
1135 *4(gk101); sod-5 (tm1146)* (**G**). For the comparison of acute locomotory speed responses
1136 between strains or conditions, red bars on the x-axis represent the time interval (6–10 minutes)
1137 used for statistical analysis. *** = $p < 0.001$, ** = $p < 0.01$, * = $p < 0.05$, ns = not significant,
1138 Mann–Whitney U test. (**H**) Hypothetical model of the role of mitochondria in response to toxic
1139 levels of H_2S. In this model, mitochondria play a dual role in H_2S-evoked avoidance behavior.
1140 A transient burst of mitochondrial ROS triggered by high H_2S levels initiates locomotory

1141 avoidance, whereas sustained ROS elevation activates stress-responsive pathways, including
1142 HIF-1, NRF2/SKN-1, and DAF-16/FOXO, promoting adaptation to prolonged H_2S exposure.
1143
1144 **Figure supplement legends**
1145 **Figure 2—figure supplement 1. Acute avoidance response to H_2S is regulated by cGMP**
1146 **signaling**
1147 (**A–H**) Fraction of animals undergoing reorientation movements (omega turns, left) or
1148 backward locomotion (reversals, right) during a switch from 7% O_2 to 150 ppm H_2S balanced
1149 with 7% O_2 for animals of the indicated genotype: WT and *daf-19(m86)* (**A, B**); WT and *dyf-*
1150 *3(m185)* (**C, D**); WT and *dyf-7(m539)* (**E, F**); WT, *daf-11(m47)*, and *tax-4(p678)* (**G, H**).
1151
1152 **Figure 2—figure supplement 2. Acute response to H_2S is regulated by *daf-11* signaling in**
1153 **ASJ neurons**
1154 (**A**) The detailed expression pattern of each promoter used to express *daf-11* genomic DNA.
1155 Promoters shown in green rescued the *daf-11(m47)* mutant phenotype. (**B–D**) Locomotory
1156 speed responses to a switch from 7% O_2 to 150 ppm H_2S balanced with 7% O_2 for animals of
1157 the indicated genotype: WT, *daf-11(m47)*, and transgenic *daf-11* mutants expressing *daf-11*
1158 genomic DNA in different subsets of neurons. Red bars on the x-axis represent two intervals
1159 (4–5 minutes and 11–12 minutes, labeled a and b, respectively) used for statistical analysis. *
1160 = $p < 0.05$, ns = not significant, Mann–Whitney U test. (**E**) Calcium transients evoked in ASJ
1161 neurons of WT animals in response to a switch from 7% O_2 to 3% CO_2 balanced with 7% O_2
1162 for animals (N=16).
1163
1164 **Figure 3—figure supplement 1. Insulin, TGF-β, and O_2 signaling modulate locomotory**
1165 **response to H_2S**
1166 (**A–C**) Locomotory speed responses to a switch from 7% O_2 to 150 ppm H_2S balanced with 7%
1167 O_2 for animals of the indicated genotype: WT and *nhr-49(nr2041)* (**A**); WT and *tax-6(ok2065)*
1168 (**B**); WT and *cnb-1(ok276)* (**C**). (**D–F**) Locomotory responses to a switch from 7% O_2 to 150

1169 ppm H_2S balanced with 7% O_2 for WT and *daf-2(e1370)*, including locomotory speed (**D**),
1170 reorientation (omega turns) (**E**), and reversal (**F**). WT and *daf-2* mutants were maintained at
1171 15°C. L4 animals were picked and shifted to 25°C until day-one adults, then assayed at room
1172 temperature. (**G–I**) Locomotory responses to a switch from 7% O_2 to 150 ppm H_2S balanced
1173 with 7% O_2 for WT and *gcy-9(tm7632)*, including locomotory speed (**G**), reorientation (omega
1174 turns) (**H**), and reversal (**I**). (**J**) Locomotory speed responses to a switch from 7% O_2 to 150
1175 ppm H_2S balanced with 7% O_2 for WT animals and wild isolate CB4856. (**K**) Optogenetic
1176 stimulation of RMG neurons using channelrhodopsin-2 (ChR2). ChR2 was expressed in RMG
1177 neurons using the Cre-LoxP system (Macosko et al., 2009). Blue light was delivered as soon as
1178 the assay was initiated at 7% O_2. Locomotory speed responses to a switch from 7% O_2 to 150
1179 ppm H_2S balanced with 7% O_2 were recorded for day-one adults grown for 16 hours in the
1180 presence or absence of ATR. (**L**) Locomotory speed responses to a switch from 7% O_2 to 150
1181 ppm H_2S balanced with 7% O_2, following activation of O_2 sensing neurons by expressing a
1182 gain-of-function allele of *pkc*-1 in O_2 sensory neurons under *gcy-37* promoter. For the
1183 comparison of acute locomotory speed responses between strains or conditions, red bars on the
1184 x-axis represent two intervals (4–5 minutes and 11–12 minutes, indicated with red bars on the
1185 x-axis) for statistical analysis. **** = $p < 0.0001$, *** = $p < 0.001$, ** = $p < 0.01$, ns = not
1186 significant, Mann–Whitney U test.
1187
1188 **Figure 4—figure supplement 1. Transcriptome reprogramming induced by H_2S exposure**
1189 (**A**) Venn diagram displaying the number of differentially expressed genes with adjusted *p*
1190 value <1e-10 in WT animals exposed to 50 ppm H_2S balanced with 7% O_2 for 1, 2, or 12 hours.
1191 (**B, C**) Significantly enriched GO categories for differentially expressed genes with adjusted *p*
1192 value <1e-10 in WT animals exposed to 50 ppm (**B**) or 150 ppm (**C**) H_2S balanced with 7% O_2
1193 for 2 hours. (**D, E**) Volcano plots showing the differentially expressed genes with adjusted *p*
1194 value <1e-10 in WT animals exposed to 50 ppm (**D**) or 150 ppm (**E**) H_2S balanced with 7% O_2
1195 for 2 hours. A set of genes involved in H_2S detoxification, cysteine metabolism and stress
1196 response are highlighted in red. (**F, G**) The number of HIF-1(**F**) and SKN-1(**G**) target genes

1197 induced by 50 ppm or 150 ppm H_2S exposure for 1 hour, 2 hours or 12 hours in WT animals,
1198 with adjusted *p* value < 1e-30. (**H–J**) Venn diagrams displaying the number of differentially
1199 expressed genes (adjusted *p* value <1e-10) in WT animals under the indicated conditions:
1200 animals exposed to 50 ppm or 150 ppm H_2S for 1hour (**H**); 2 hours (**I**); and 12 hours (**J**). (**K,**
1201 **L**) Volcano plots showing the differentially expressed genes (adjusted *p* value <1e-10) in WT
1202 animals that were exposed to either 50 ppm (**K**) or 150 ppm (**L**) H_2S balanced with 7% O_2 for
1203 12 hours. A set of genes involved in H_2S detoxification, cysteine metabolism and stress
1204 response are highlighted in red.
1205
1206 **Figure 5—figure supplement 1. Acute response to H_2S is modulated by HIF-1 signaling**
1207 (**A, B**) Fraction of WT and *egl-9(sa307)* animals undergoing reorientation movements (omega
1208 turns) (**A**) or backward locomotion (reversals) (**B**) during a switch from 7% O_2 to 150 ppm H_2S
1209 balanced with 7% O_2. (**C, D**) Locomotory speed responses to a switch from 7% O_2 to 1% O_2
1210 for WT and *egl-9(sa307)* (**C**); WT, *hif-1(ia4)*, and *semo-1(yum2889)* (**D**). (**E**) HIF-1 signaling
1211 regulates the H_2S mitochondrial detoxification pathway. The detoxification enzyme SQRD-1
1212 (sulfide:quinone oxidoreductase) oxidizes H_2S, donating electrons to ubiquinone (uq), and
1213 rhodoquinone (rq) of the mitochondrial electron transport chain (ETC). ETHE-1 (persulfide
1214 dioxygenase) oxidizes sulfur compounds to sulfite. (**F–I**) Fraction of animals undergoing
1215 reorientation movements (omega turns, F and H) or backward locomotion (reversals, G and I)
1216 during a switch from 7% O_2 to 150 ppm H_2S balanced with 7% O_2 for the indicated genotypes:
1217 WT and *sqrd-1(tm3378)* (**F, G**)*;* and WT and *ethe-1(yum2895)* (**H, I**). (**J**) Locomotory speed
1218 responses to a switch from 7% O_2 to 1% O_2 for WT, *sqrd-1(tm3378)*, and *ethe-1(yum2895)*. (**K,**
1219 **L**) Fraction of WT, *cysl-1(ok762), cysl-2(ok3516)*, and *cysl-3(yum4)* animals undergoing
1220 reorientation movements (omega turns, K) or backward locomotion (reversals, L) during a
1221 switch from 7% O_2 to 150 ppm H_2S balanced with 7% O_2. (**M**) Locomotory speed responses to
1222 a switch from 7% O_2 to 1% O_2 for WT, *cysl-1(ok762), cysl-2(ok3516)*, and *cysl-3(yum4)*
1223 animals. (**N**) Locomotory speed responses to a switch from 7% O_2 to 150 ppm H_2S balanced
1224 with 7% O_2 for WT and *semo-1(yum2889).* (**O, P**) Fraction of animals undergoing reorientation

1225 (omega turns, **O**) or backward locomotion (reversals, **P**) in response to a switch from 7% O_2 to
1226 150 ppm H_2S balanced with 7% O_2. Comparisons of acute locomotory responses between
1227 strains were performed using two intervals (4–5 minutes and 11–12 minutes, indicated with red
1228 bars on the x-axis) for statistical analysis. *** = $p < 0.001$, ns = not significant, Mann–Whitney
1229 U test.
1230
1231 **Figure 6—figure supplement 1. Labile iron pool sustains the locomotory activity in H_2S**
1232 (**A–D**) Volcano plots showing the relative expression of the genes involved in the regulation of
1233 iron homeostasis (*ftn-1*, *ftn-2*, and *smf-3*) in WT animals under the following conditions: 1-hour
1234 exposure in 50 ppm H_2S balanced with 7% O_2 (**A**); 1-hour exposure in 150 ppm H_2S balanced
1235 with 7% O_2 (**B**); 12-hour exposure in 50 ppm H_2S balanced with 7% O_2 (**C**); and 12-hour
1236 exposure in 150 ppm H_2S balanced with 7% O_2 (**D**). (**E, F**) Locomotory speed responses to a
1237 switch from 7% O_2 to 1% O_2 for animals of the indicated genotype or treatment: WT, and two
1238 independent transgenic lines overexpressing *ftn-1* genomic DNA under its own promoter (#1
1239 and #2) (**E**); WT animals, WT animals treated with 100 μM 2,2′-Bipyridyl (BP), and WT
1240 animals treated with 5 mg/ml ferric ammonium citrate (FAC) for 16 hours (**F**). Red bar on the
1241 x-axis represents one-minute time interval (3–4 minutes) used for statistical analysis. * = $p <$
1242 0.05, ns = not significant, Mann–Whitney U test. (**G, H**) Fraction of animals undergoing
1243 reorientation movements (omega turns) (**G**) or backward locomotion (reversals) (**H**) during a
1244 switch from 7% O_2 to 150 ppm H_2S balanced with 7% O_2 for animals of the indicated genotypes
1245 WT, *smf-3(ok1305)*, and *ftn-1(ok3625)*. (**I, J**) Fraction of animals undergoing reorientation
1246 movements (omega turns) (**I**) or backward locomotion (reversals) (**J**) during a switch from 7%
1247 O_2 to 150 ppm H_2S balanced with 7% O_2 for WT animals, WT animals pretreated with either
1248 100 μM 2,2′-Bipyridyl (BP) or with 5 mg/ml ferric ammonium citrate (FAC) in the presence of
1249 food for 16 hours.
1250
1251 **Figure 7—figure supplement 1. Mitochondrial function is required for acute response to**
1252 **H_2S**

1253 (**A–D**) Fraction of animals undergoing reorientation movements (omega turns) or backward
1254 locomotion (reversals) during a switch from 7% O_2 to 150 ppm H_2S balanced with 7% O_2 for
1255 the indicated genotype or treatment: WT and *clk-1(qm30)* (**A, B**); WT and *mev-1(kn1)* (**C, D**).
1256 (**E**) Locomotory speed responses to a switch from 7% O_2 to 1% O_2 for WT, *sod-2(ok1030);* and
1257 *sod-3(tm760)*. (**F, G**) Fraction of animals undergoing reorientation movements (omega turns,
1258 **F**) or backward locomotion (reversals, **G**) during a switch from 7% O_2 to 150 ppm H_2S balanced
1259 with 7% O_2 for WT and *sod-1(tm783); sod-2(ok1030); sod-3(tm760); sod-4(gk101); sod-5*
1260 *(tm1146*). (**H**) Locomotory response to acute near UV exposure for WT and *sod-1(tm783); sod-*
1261 *2(ok1030); sod-3(tm760); sod-4(gk101); sod-5 (tm1146*) before and after 30 minutes of
1262 exposure to 150ppm H_2S.
1263
1264 **Figure 1—Video 1. The locomotory response of WT animals to H_2S**
1265 An 8x accelerated video clip (original length: 16 minutes) showing WT (N2) animals exposed
1266 to 7% O_2 for 2 minutes, followed by 11 minutes in 150 ppm H_2S, and then returned to 7% O_2.
1267 The H_2S exposure segment is highlighted and begins at the 15-second mark, corresponding to
1268 2 minutes in the original recording.

Figure 1

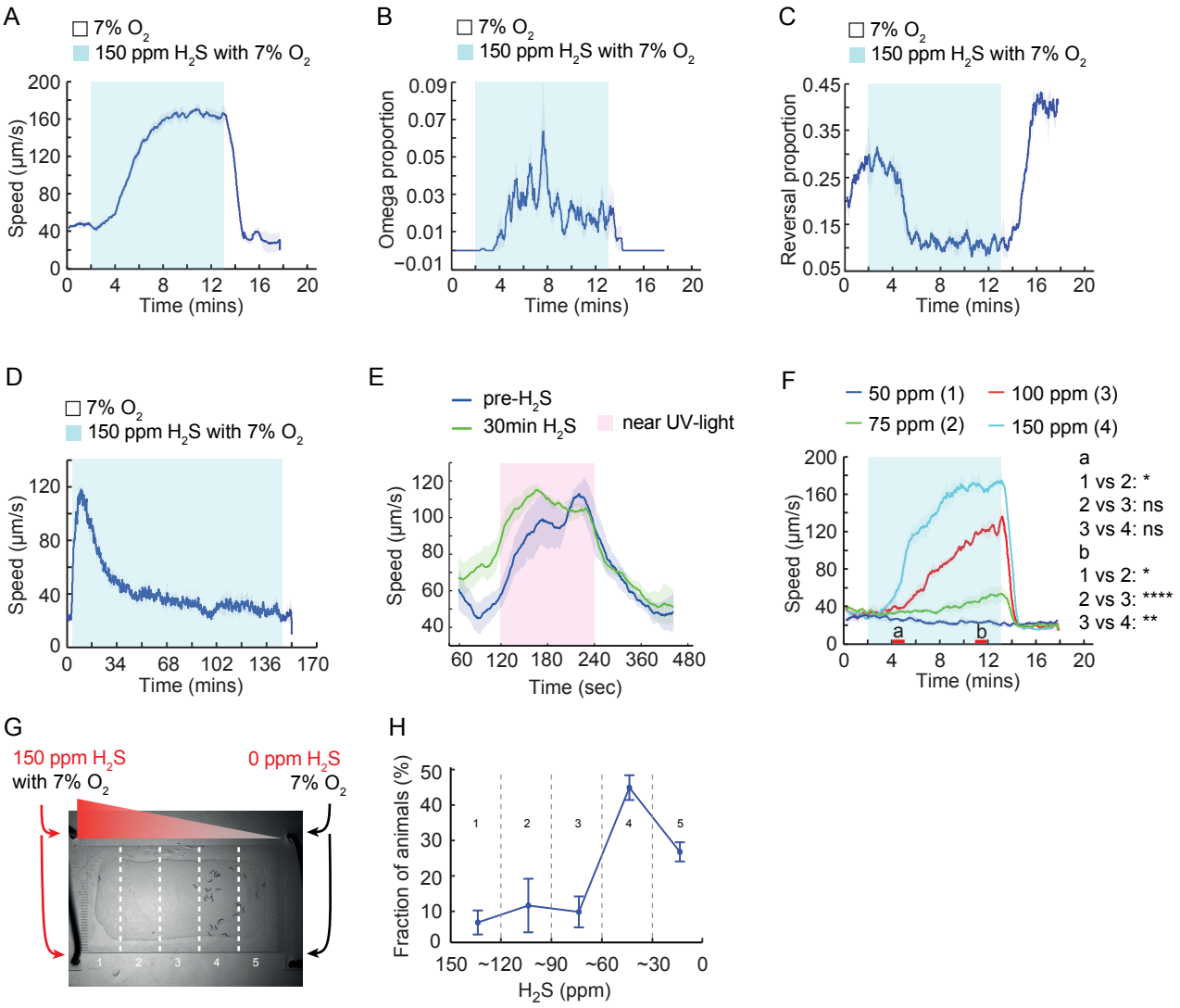
A
7% O2
150 ppm H2S with 7% O2
Speed (µm/s)
Time (mins)
B
7% O2
150 ppm H2S with 7% O2
Omega proportion
Time (mins)
C
7% O2
150 ppm H2S with 7% O2
Reversal proportion
Time (mins)
D
7% O2
150 ppm H2S with 7% O2
Speed (µm/s)
Time (mins)
E
pre-H2S
30min H2S
near UV-light
Speed (µm/s)
Time (sec)
F
50 ppm (1)
75 ppm (2)
100 ppm (3)
150 ppm (4)
Speed (µm/s)
Time (mins)
a
1 vs 2: *
2 vs 3: ns
3 vs 4: ns
b
1 vs 2: *
2 vs 3: ****
3 vs 4: **
G
150 ppm H2S
with 7% O2
0 ppm H2S
7% O2
H
Fraction of animals (%)
H2S (ppm)

Figure 2

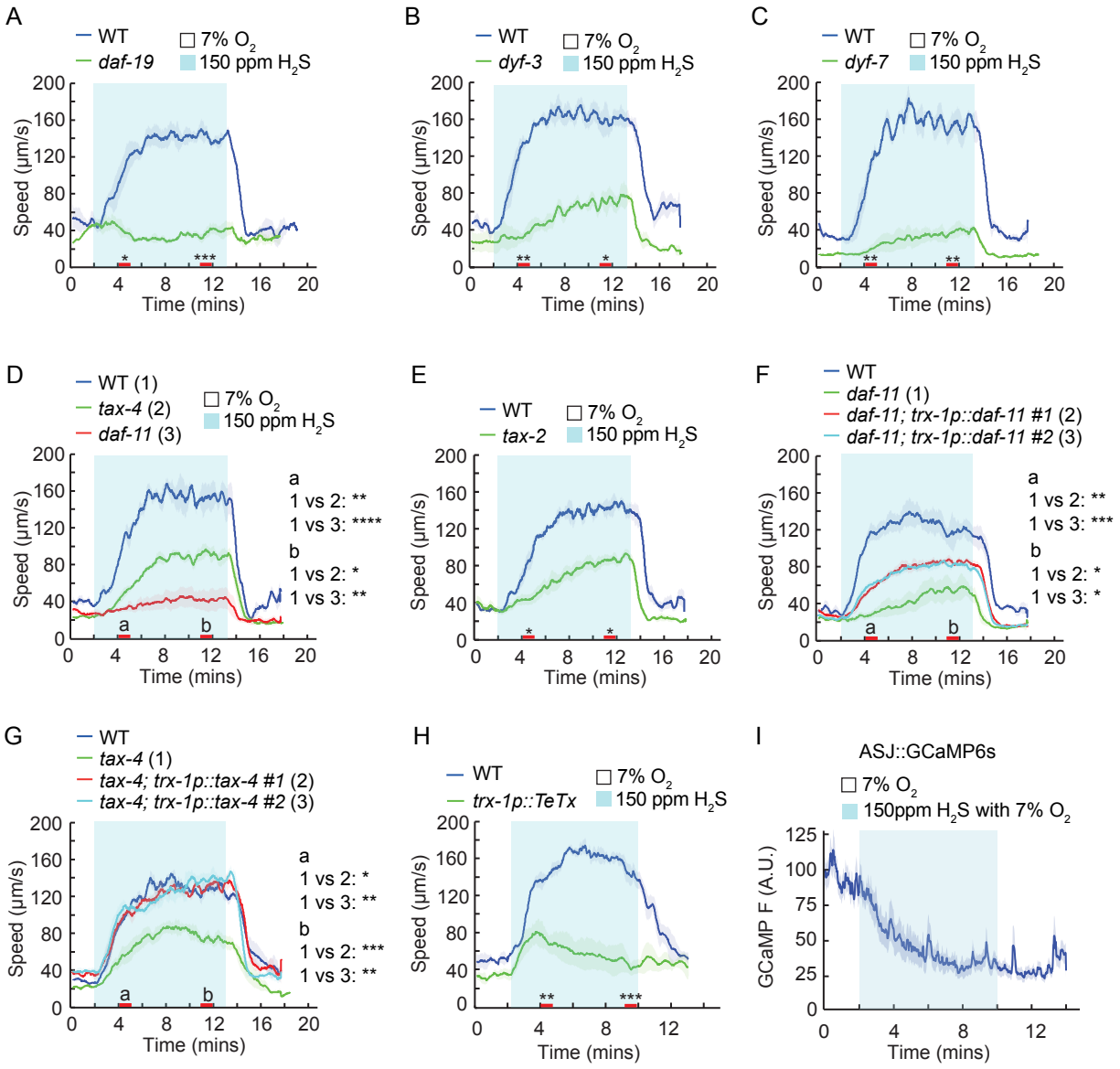
A
WT
daf-19
7% O2
150 ppm H2S
Speed (µm/s)
Time (mins)
B
WT
dyf-3
7% O2
150 ppm H2S
C
WT
dyf-7
7% O2
150 ppm H2S
D
WT (1)
tax-4 (2)
daf-11 (3)
7% O2
150 ppm H2S
a
1 vs 2: **
1 vs 3: ****
b
1 vs 2: *
1 vs 3: **
E
WT
tax-2
7% O2
150 ppm H2S
F
WT
daf-11 (1)
daf-11; trx-1p::daf-11 #1 (2)
daf-11; trx-1p::daf-11 #2 (3)
a
1 vs 2: **
1 vs 3: ***
b
1 vs 2: *
1 vs 3: *
G
WT
tax-4 (1)
tax-4; trx-1p::tax-4 #1 (2)
tax-4; trx-1p::tax-4 #2 (3)
a
1 vs 2: *
1 vs 3: **
b
1 vs 2: ***
1 vs 3: **
H
WT
trx-1p::TeTx
7% O2
150 ppm H2S
I
ASJ::GCaMP6s
7% O2
150ppm H2S with 7% O2
GCaMP F (A.U.)

Figure 3

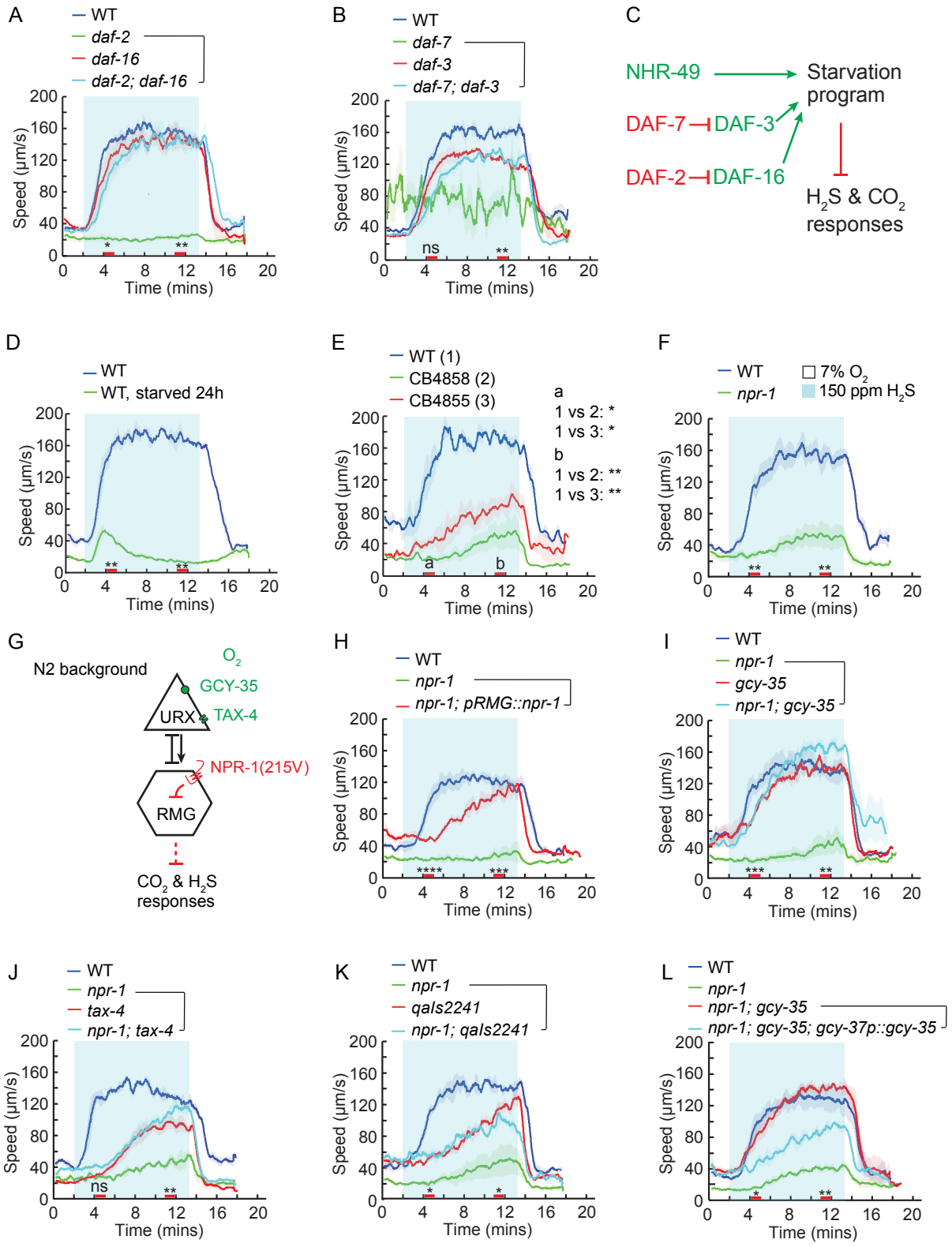
A
WT
daf-2
daf-16
daf-2; daf-16
Speed (µm/s)
Time (mins)
B
WT
daf-7
daf-3
daf-7; daf-3
ns
C
NHR-49
Starvation program
DAF-7
DAF-3
DAF-2
DAF-16
H2S & CO2 responses
D
WT
WT, starved 24h
E
WT (1)
CB4858 (2)
CB4855 (3)
a
1 vs 2: *
1 vs 3: *
b
1 vs 2: **
1 vs 3: **
F
WT
npr-1
7% O2
150 ppm H2S
G
N2 background
O2
GCY-35
TAX-4
URX
NPR-1(215V)
RMG
CO2 & H2S responses
H
WT
npr-1
npr-1; pRMG::npr-1
I
WT
npr-1
gcy-35
npr-1; gcy-35
J
WT
npr-1
tax-4
npr-1; tax-4
K
WT
npr-1
qaIs2241
npr-1; qaIs2241
L
WT
npr-1
npr-1; gcy-35
npr-1; gcy-35; gcy-37p::gcy-35

Figure 4

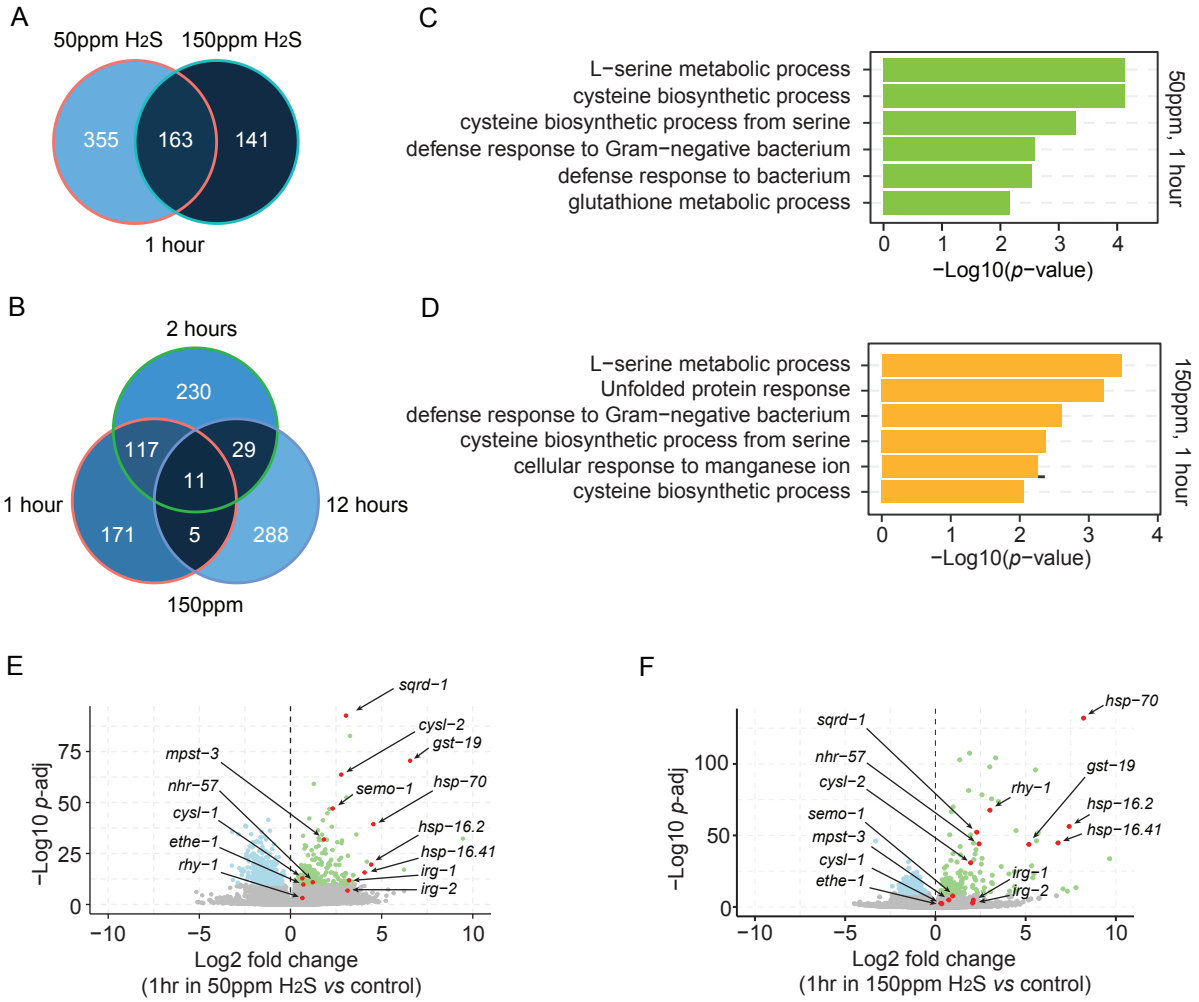
A
50ppm H2S
150ppm H2S
355
163
141
1 hour
B
2 hours
230
117
29
11
1 hour
12 hours
171
5
288
150ppm
C
L−serine metabolic process
cysteine biosynthetic process
cysteine biosynthetic process from serine
defense response to Gram−negative bacterium
defense response to bacterium
glutathione metabolic process
50ppm, 1 hour
−Log10(p−value)
D
L−serine metabolic process
Unfolded protein response
defense response to Gram−negative bacterium
cysteine biosynthetic process from serine
cellular response to manganese ion
cysteine biosynthetic process
150ppm, 1 hour
−Log10(p−value)
E
sqrd−1
cysl−2
gst−19
mpst−3
nhr−57
semo−1
hsp−70
cysl−1
hsp−16.2
ethe−1
hsp−16.41
rhy−1
irg−1
irg−2
−Log10 p-adj
Log2 fold change
(1hr in 50ppm H2S vs control)
F
hsp−70
sqrd−1
nhr−57
gst−19
cysl−2
rhy−1
semo−1
hsp−16.2
mpst−3
hsp−16.41
cysl−1
ethe−1
irg−1
irg−2
−Log10 p-adj
Log2 fold change
(1hr in 150ppm H2S vs control)

Figure 5

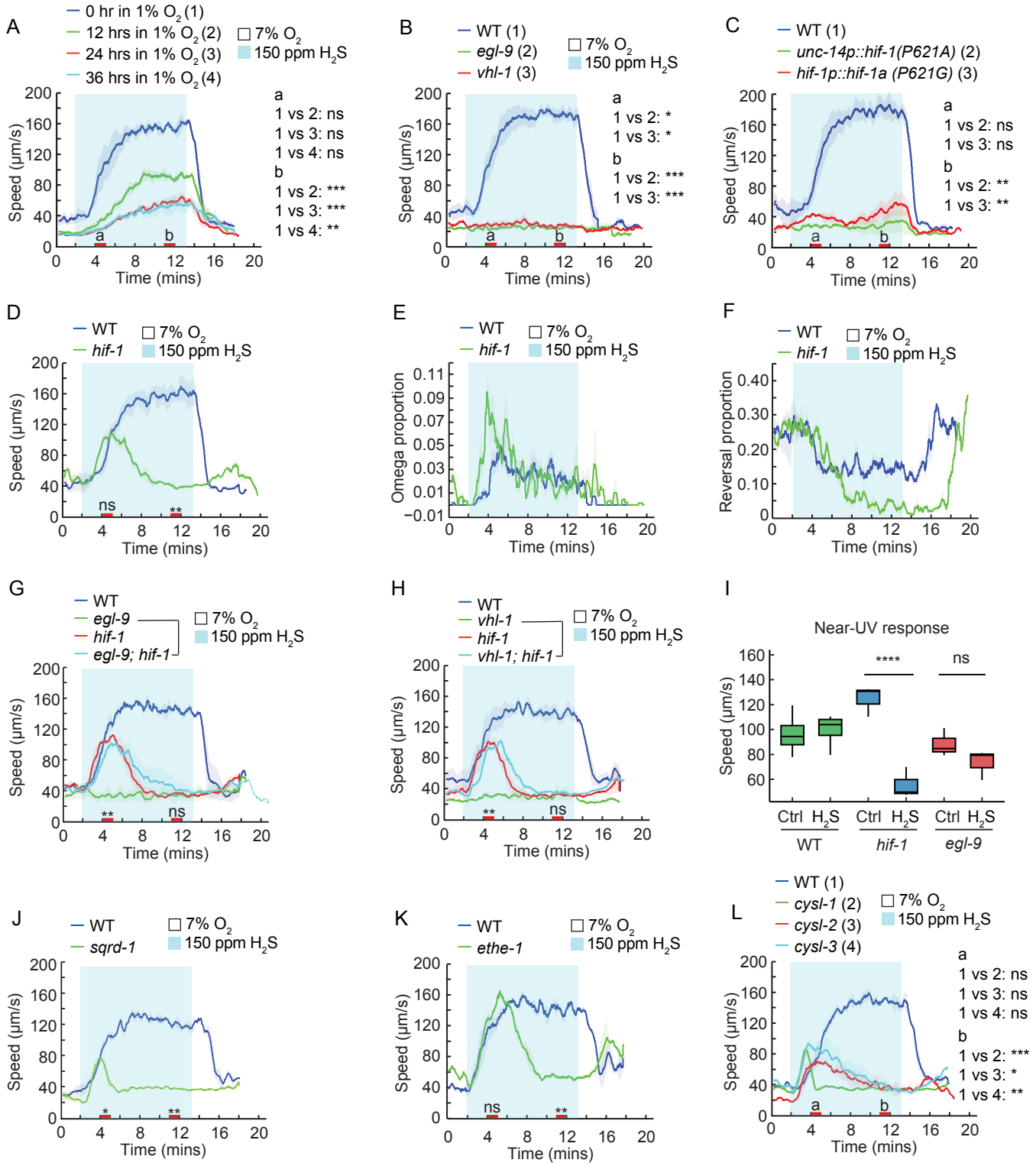
A
0 hr in 1% O2 (1)
12 hrs in 1% O2 (2)
24 hrs in 1% O2 (3)
36 hrs in 1% O2 (4)
7% O2
150 ppm H2S
a
1 vs 2: ns
1 vs 3: ns
1 vs 4: ns
b
1 vs 2: ***
1 vs 3: ***
1 vs 4: **
Speed (µm/s)
Time (mins)
B
WT (1)
egl-9 (2)
vhl-1 (3)
7% O2
150 ppm H2S
a
1 vs 2: *
1 vs 3: *
b
1 vs 2: ***
1 vs 3: ***
C
WT (1)
unc-14p::hif-1(P621A) (2)
hif-1p::hif-1a (P621G) (3)
a
1 vs 2: ns
1 vs 3: ns
b
1 vs 2: **
1 vs 3: **
D
WT
hif-1
7% O2
150 ppm H2S
ns
**
E
Omega proportion
F
Reversal proportion
G
WT
egl-9
hif-1
egl-9; hif-1
H
vhl-1
vhl-1; hif-1
I
Near-UV response
****
ns
Ctrl
H2S
WT
hif-1
egl-9
J
sqrd-1
*
K
ethe-1
L
cysl-1 (2)
cysl-2 (3)
cysl-3 (4)

Figure 6

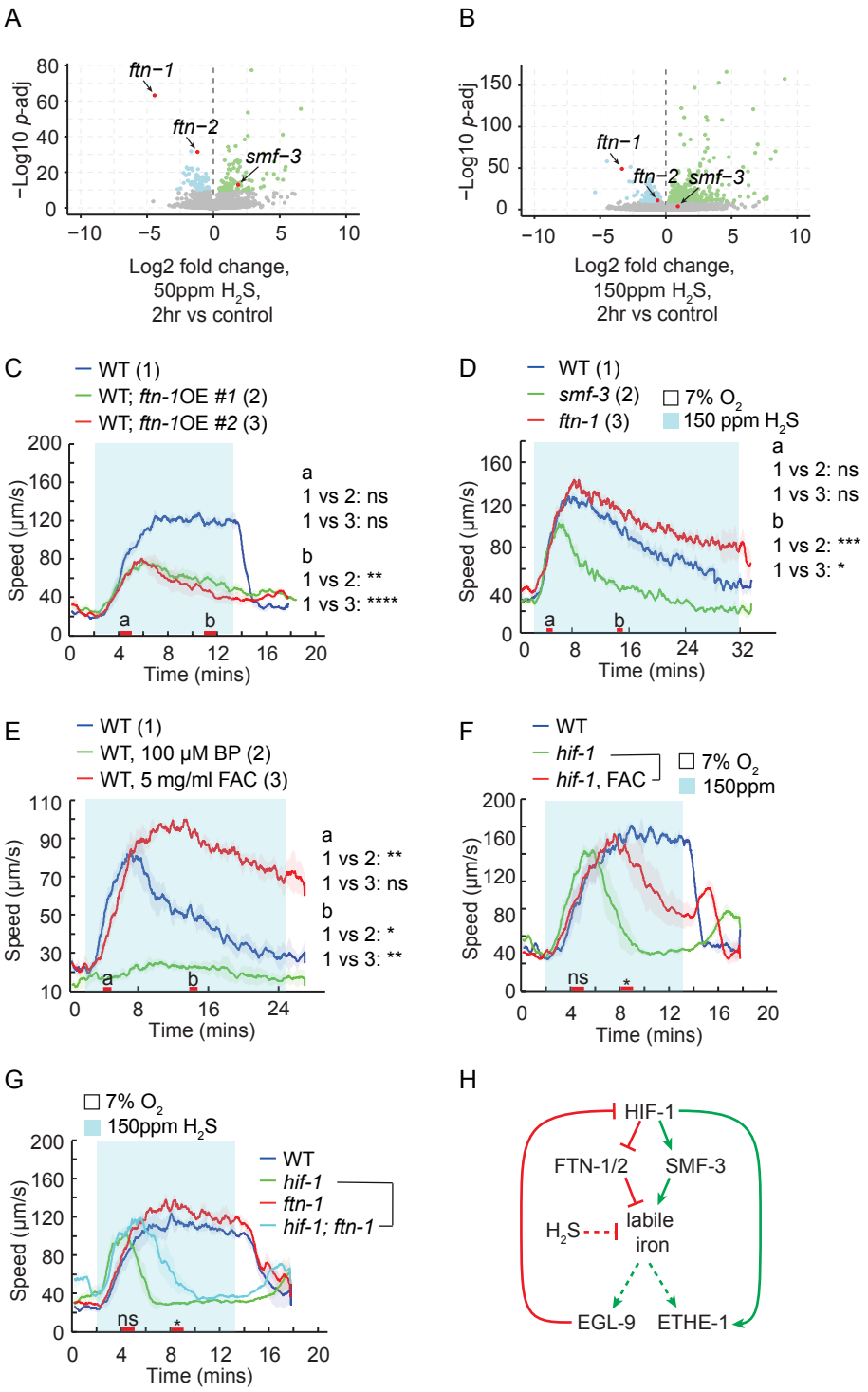
A
−Log10 p-adj
ftn−1
ftn−2
smf−3
Log2 fold change,
50ppm H2S,
2hr vs control
B
−Log10 p-adj
ftn−1
ftn−2
smf−3
Log2 fold change,
150ppm H2S,
2hr vs control
C
WT (1)
WT; ftn-1OE #1 (2)
WT; ftn-1OE #2 (3)
Speed (µm/s)
Time (mins)
a
1 vs 2: ns
1 vs 3: ns
b
1 vs 2: **
1 vs 3: ****
D
WT (1)
smf-3 (2)
ftn-1 (3)
7% O2
150 ppm H2S
Speed (µm/s)
Time (mins)
a
1 vs 2: ns
1 vs 3: ns
b
1 vs 2: ***
1 vs 3: *
E
WT (1)
WT, 100 µM BP (2)
WT, 5 mg/ml FAC (3)
Speed (µm/s)
Time (mins)
a
1 vs 2: **
1 vs 3: ns
b
1 vs 2: *
1 vs 3: **
F
WT
hif-1
hif-1, FAC
7% O2
150ppm
Speed (µm/s)
Time (mins)
ns
*
G
7% O2
150ppm H2S
WT
hif-1
ftn-1
hif-1; ftn-1
Speed (µm/s)
Time (mins)
ns
*
H
HIF-1
FTN-1/2
SMF-3
H2S
labile
iron
EGL-9
ETHE-1

Figure 7

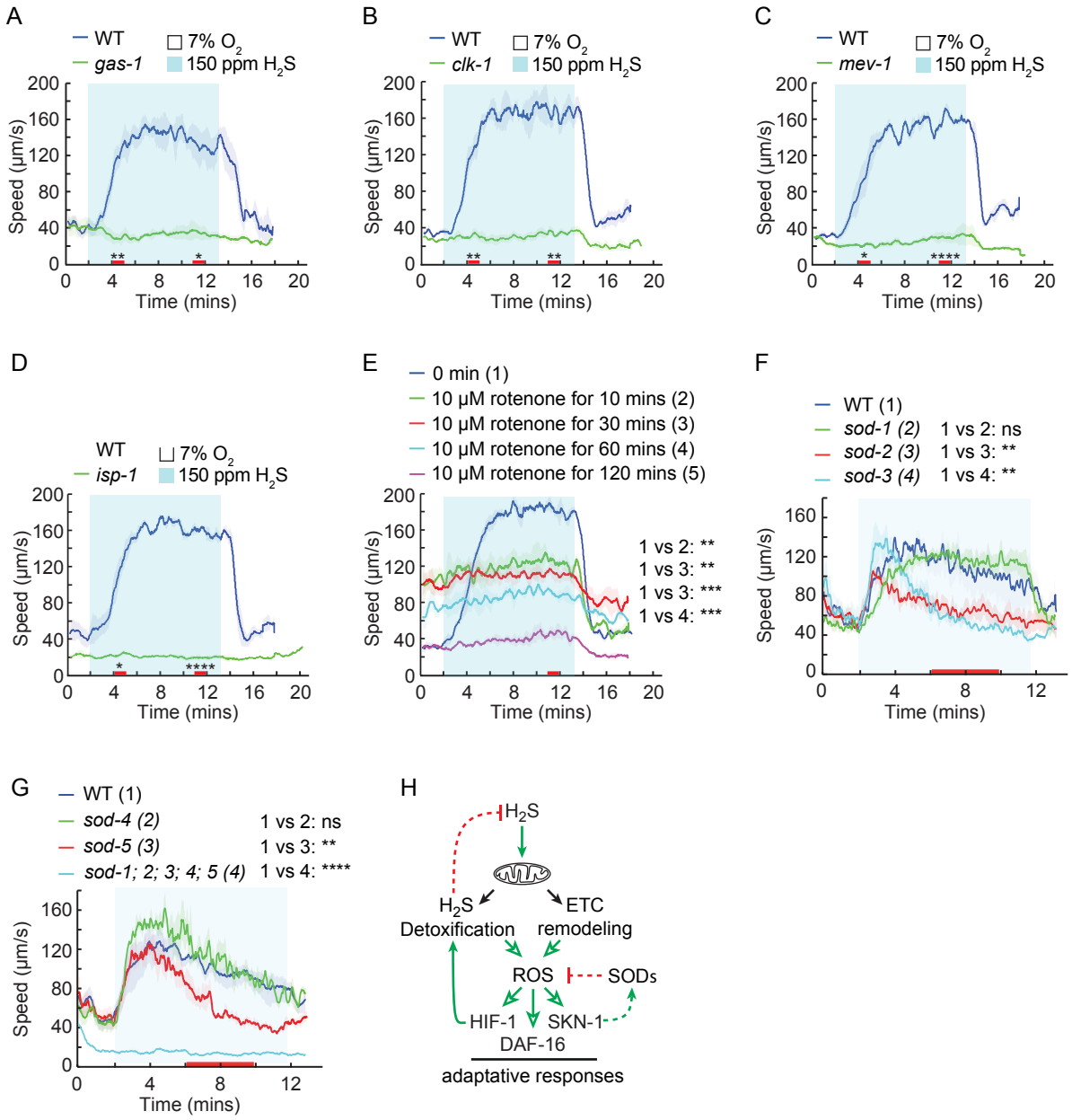
A
WT
gas-1
7% O2
150 ppm H2S
Speed (μm/s)
Time (mins)
B
WT
clk-1
7% O2
150 ppm H2S
C
WT
mev-1
7% O2
150 ppm H2S
D
WT
isp-1
7% O2
150 ppm H2S
E
0 min (1)
10 μM rotenone for 10 mins (2)
10 μM rotenone for 30 mins (3)
10 μM rotenone for 60 mins (4)
10 μM rotenone for 120 mins (5)
1 vs 2: **
1 vs 3: **
1 vs 3: ***
1 vs 4: ***
F
WT (1)
sod-1 (2) 1 vs 2: ns
sod-2 (3) 1 vs 3: **
sod-3 (4) 1 vs 4: **
G
WT (1)
sod-4 (2) 1 vs 2: ns
sod-5 (3) 1 vs 3: **
sod-1; 2; 3; 4; 5 (4) 1 vs 4: ****
H
H2S
H2S
Detoxification
ETC
remodeling
ROS
SODs
HIF-1
SKN-1
DAF-16
adaptative responses

Figure 2—figure supplement 1

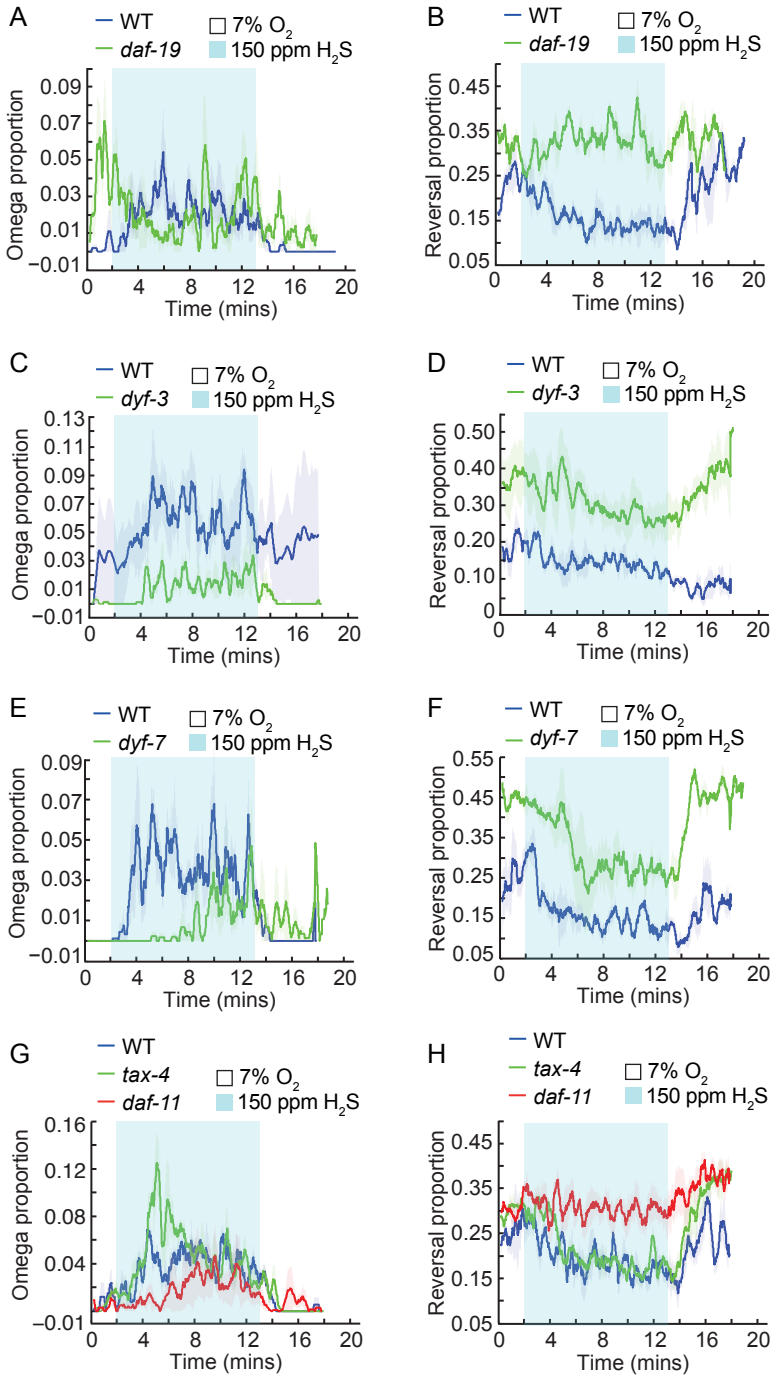

Figure 2—figure supplement 2

A

Promoter	neurons																
Pdaf-11	ASH	AWB	AWC	ASJ	ASK	ADL	ASI	ASE									
Podr-3	ASH	AWB	AWC						ADF	AWA							
Podr-1		AWB	AWC	ASJ	ASK		ASI										
Pflp-21	ASH					ADL	ASI	ASE			FLP	URA	RMG	MC	M2	M4	
Pgpa-11	ASH					ADL											
Psra-6	ASH						ASI										PVQ
Ptrx-1				ASJ													

B

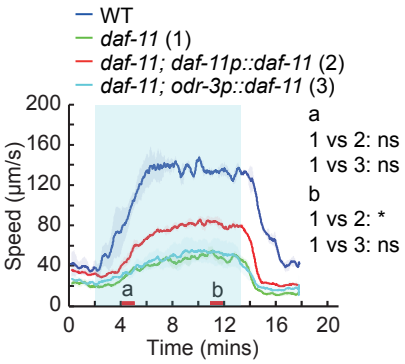

C

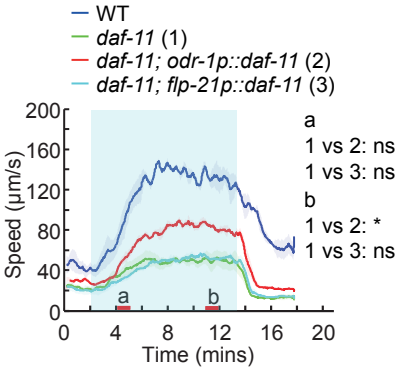

D

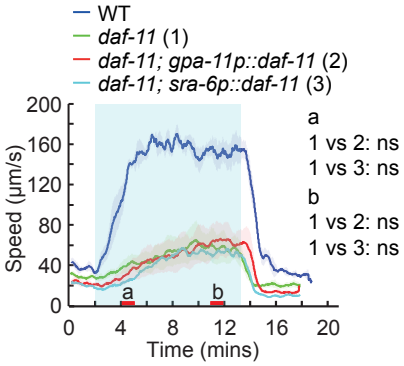

E

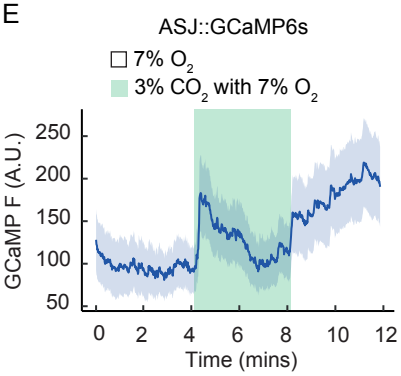

Figure 3—figure supplement 1

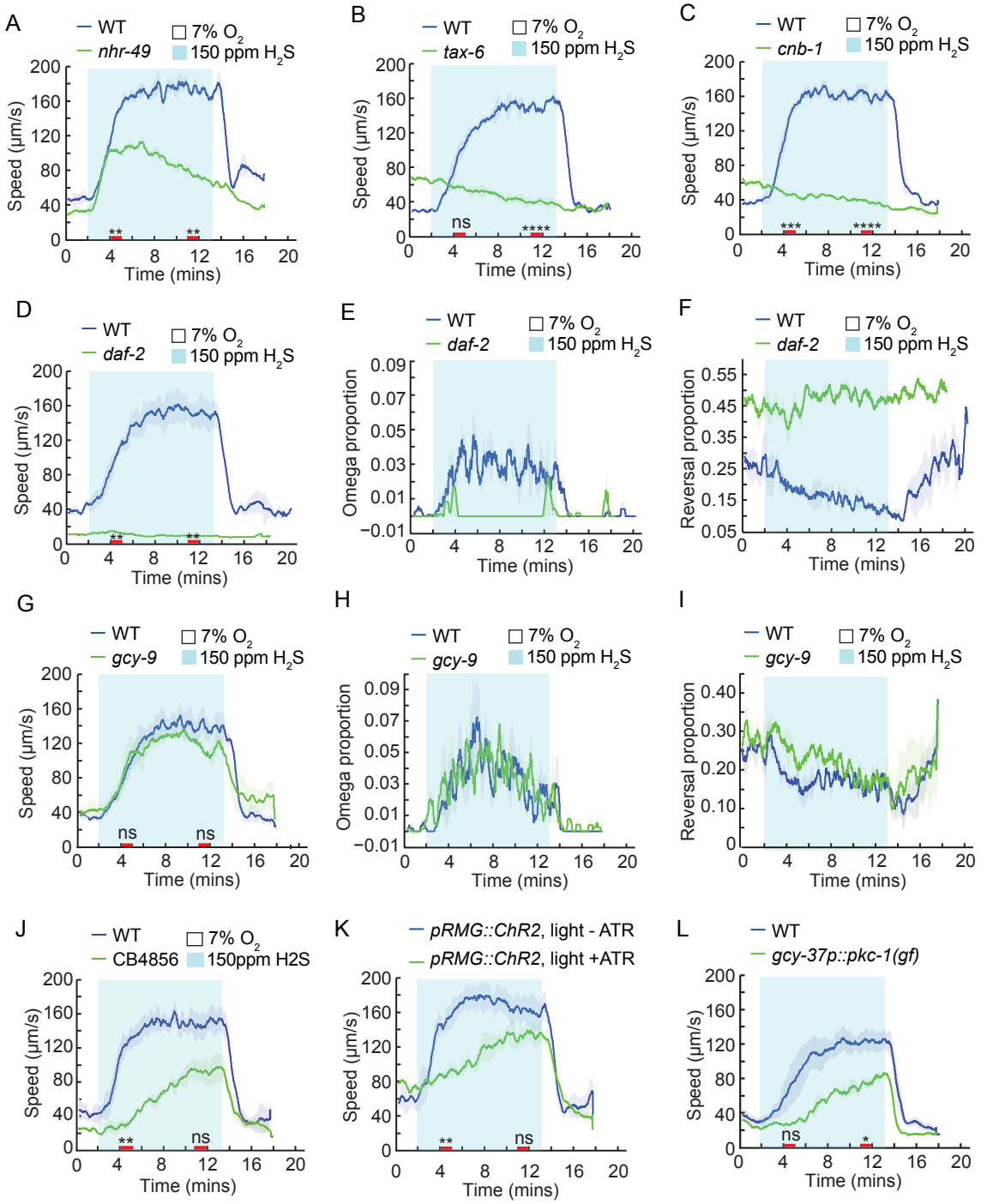

Figure 4—figure supplement 1

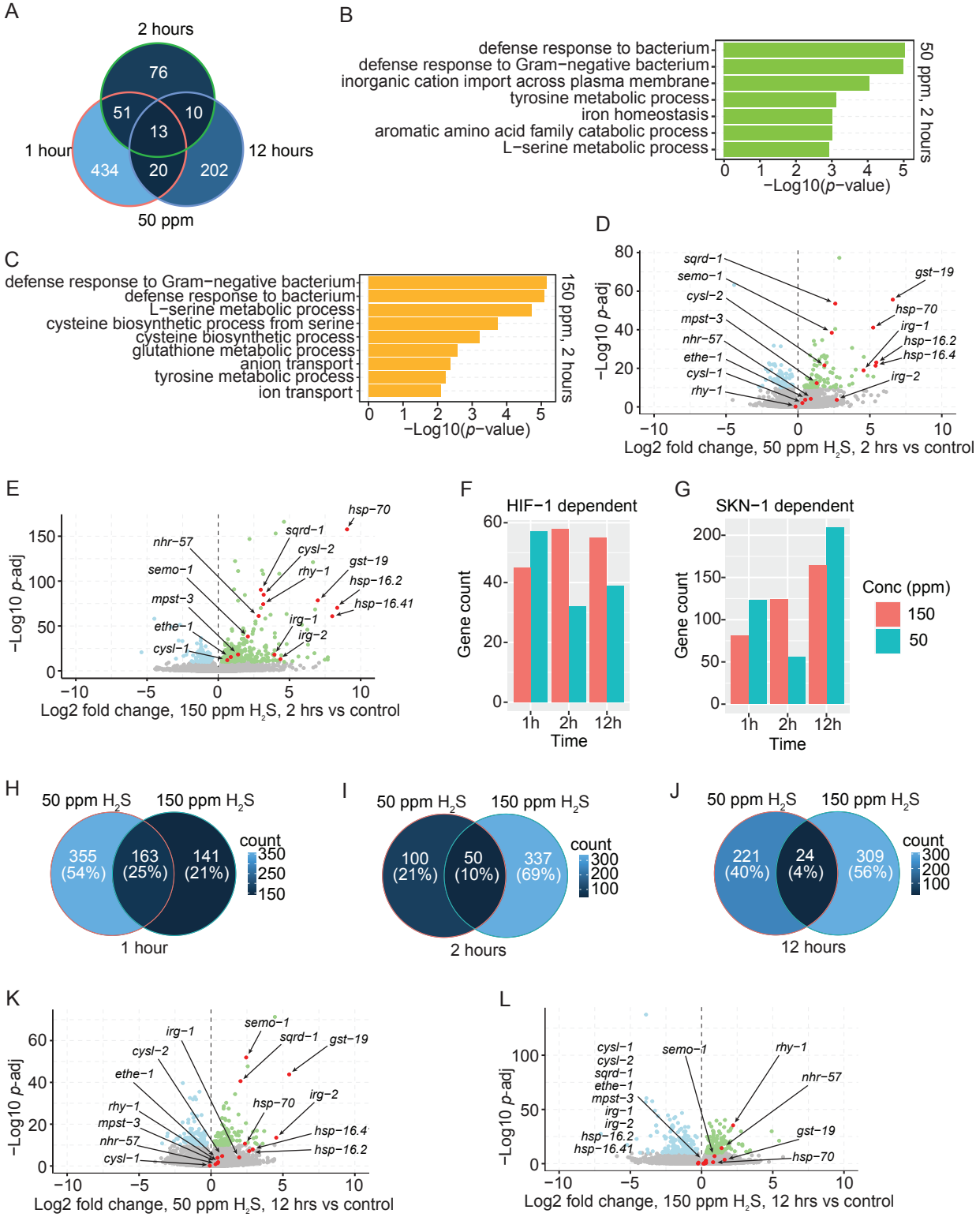

Figure 5—figure supplement 1

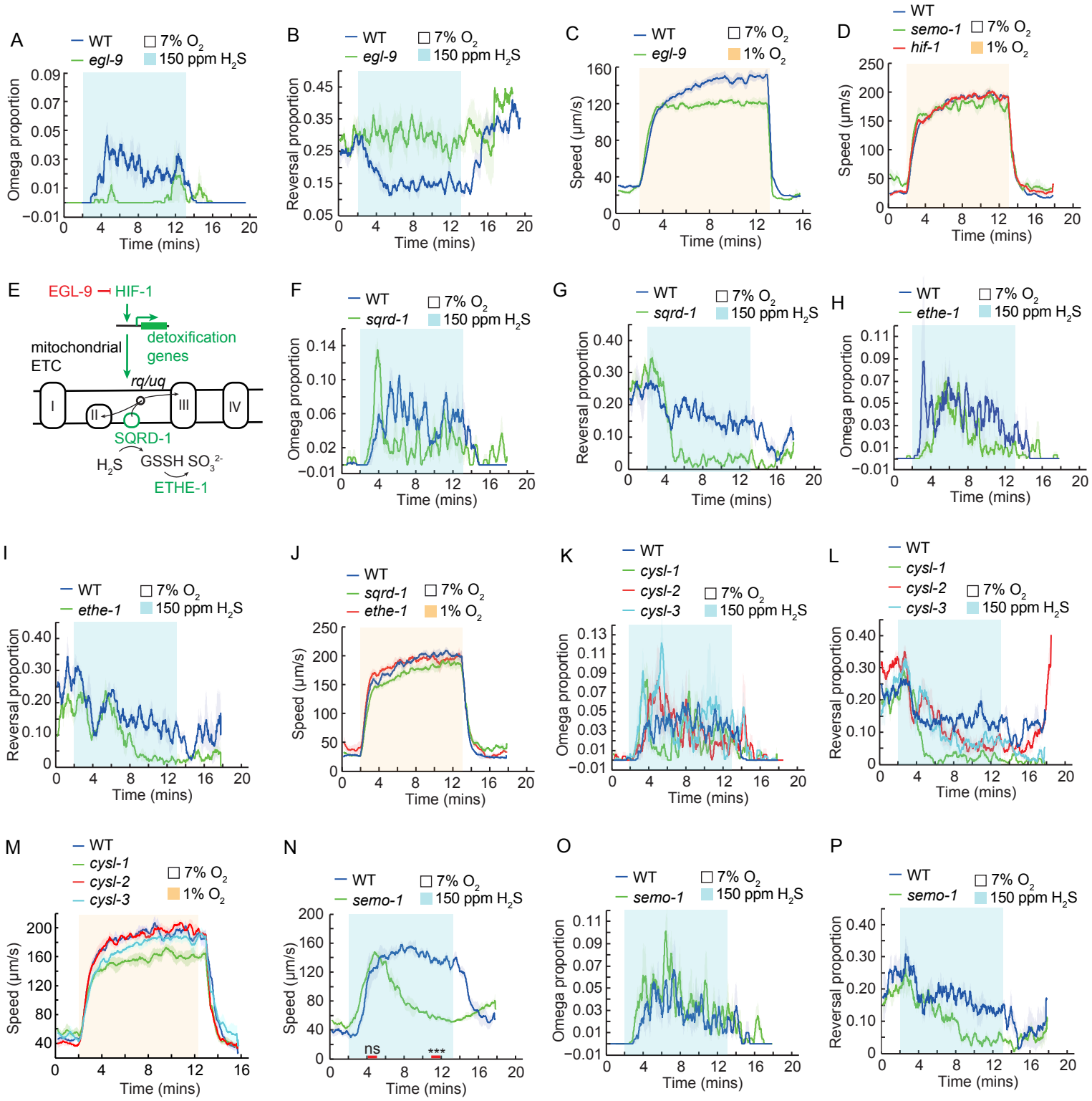

Figure 6—figure supplement 1

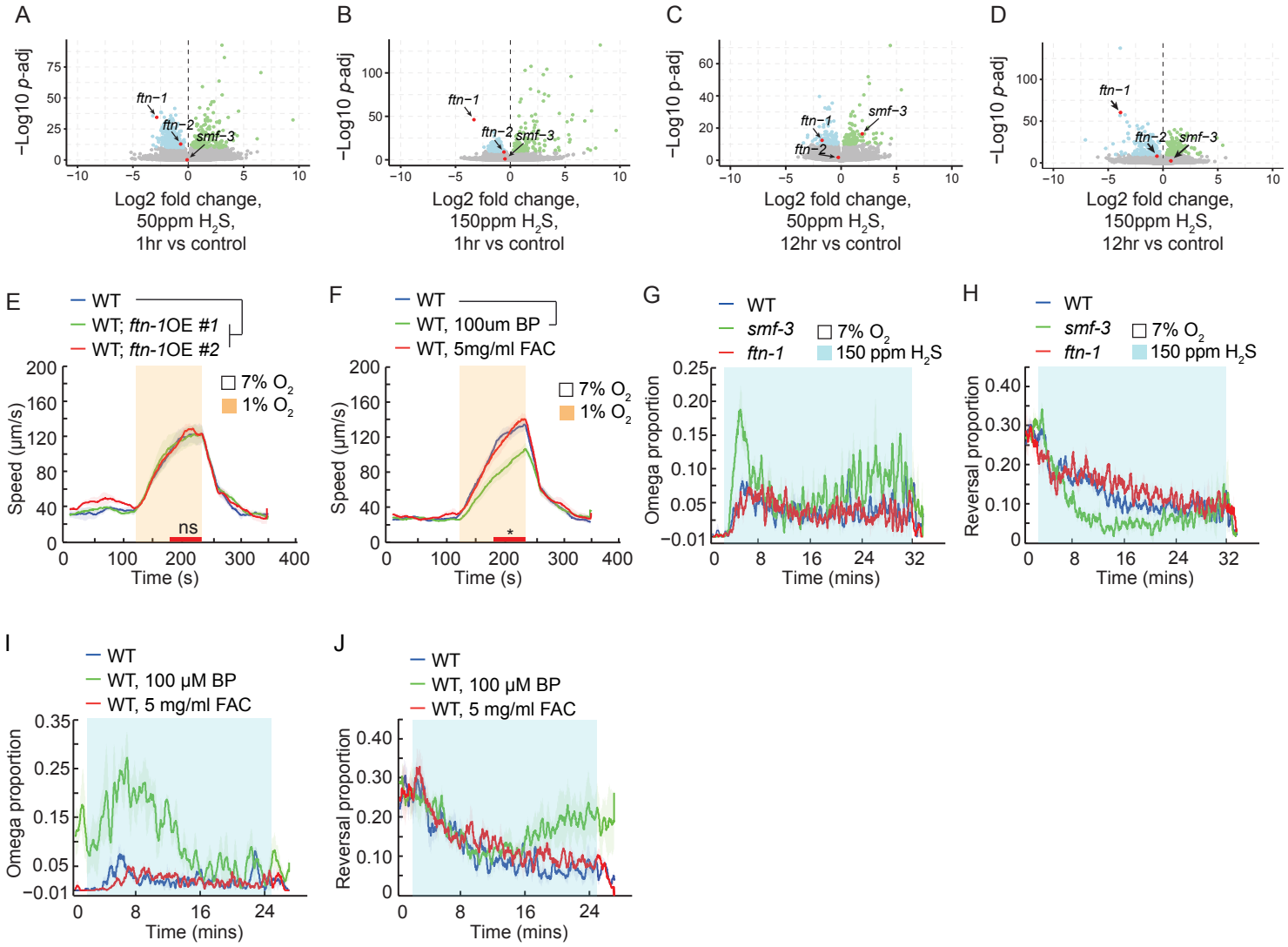
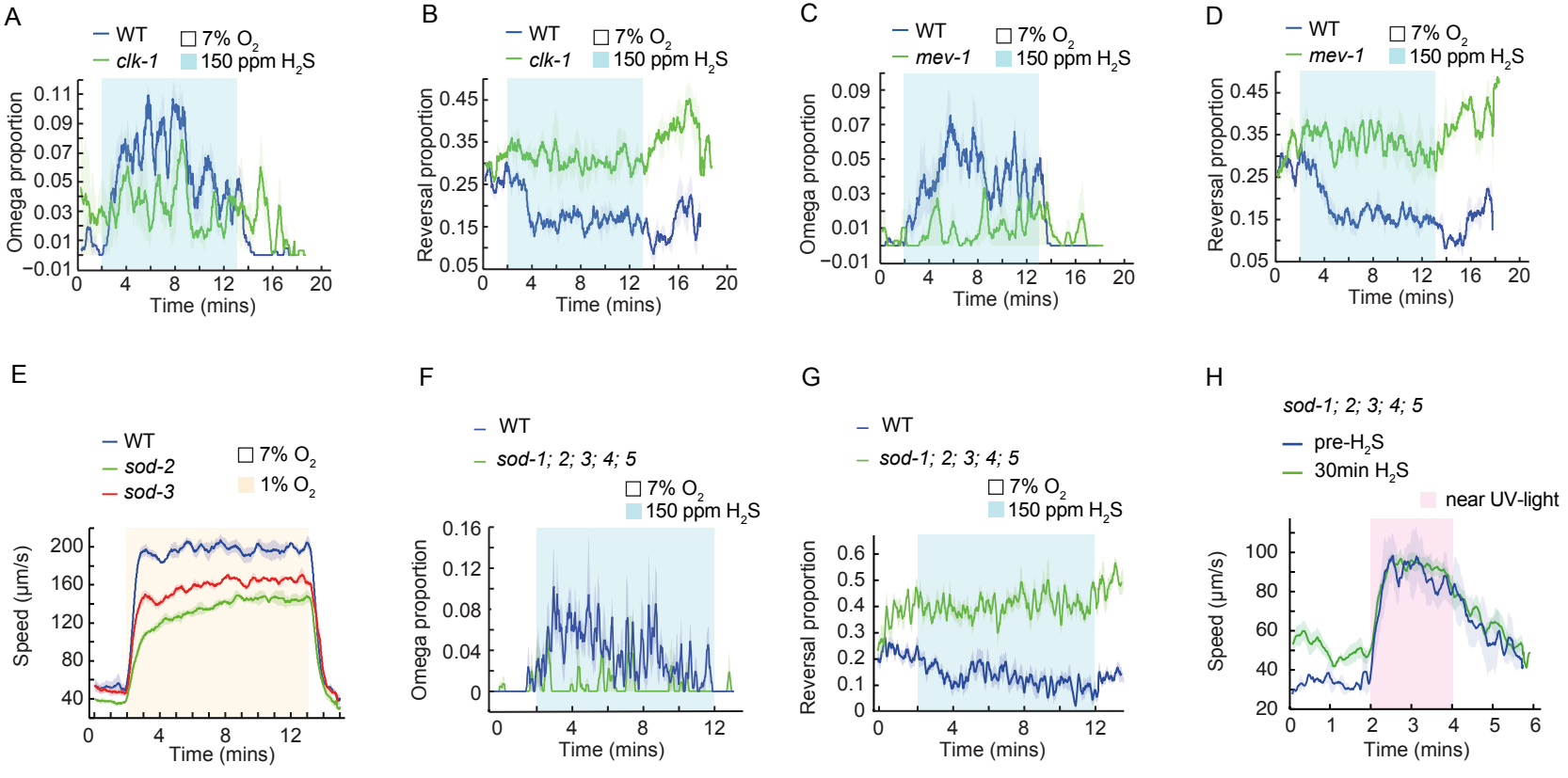
Figure 7—figure supplement 1